FB-MOAC: A Reinforcement Learning Algorithm for Forward-Backward Markov Decision Processes

Anonymous authors
Paper under double-blind review

Abstract

Reinforcement learning (RL) algorithms are effective in solving problems that can be modeled as Markov decision processes (MDPs). They primarily target forward MDPs whose dynamics evolve over time from an initial state. However, several important problems in stochastic control and network systems, among others, exhibit both a forward and a backward dynamics. As a consequence, they cannot be expressed as a standard MDP, thereby calling for a novel theory for RL in this context. Accordingly, this work introduces the concept of Forward-Backward Markov Decision Processes (FB-MDPs) for multi-objective problems and develops a novel theoretical framework to characterize their optimal solutions. Moreover, it introduces the FB-MOAC algorithm that employs a step-wise forward-backward mechanism to obtain optimal policies with guaranteed convergence and a competitive rate with respect to standard approaches in RL. FB-MOAC is finally evaluated on three use cases in the context of mathematical finance, mobile resource management, and edge computing. The obtained results show that FB-MOAC outperforms the state of the art across different metrics, highlighting its ability to learn and maximize rewards.

1 Introduction

Reinforcement Learning (RL) is a very important field of artificial intelligence, as it enables agents to learn from experience and adapt to complex, dynamic environments (Mnih et al., 2013; Lillicrap et al., 2016; Schulman et al., 2017b). Moreover, recent breakthroughs in deep learning have led to solutions that surpass human performance in a wide variety of challenges. As a result, deep reinforcement learning has lately emerged as a combination of these two fields, with successful applications in different use cases (Mnih et al., 2015; Jaderberg et al., 2018; Rigoli et al., 2021).

Existing RL algorithms mainly address sequential decision-making problems modeled as a forward Markov decision process (MDP) or controlled forward dynamics (Zare et al., 2023). However, there are several sequential tasks whose environment cannot be exclusively captured by this type of dynamics, as they also encompass states evolving backwards in time (Lai et al., 2020; Wang et al., 2021). Such backward dynamics describe a trajectory in a reverse chronological order, wherein the future affects the past. Even further, there are environments exhibiting *both* controlled forward and backward dynamics at the same time (Ji et al., 2022a; Zhang, 2022), namely, as a forward-backward MDP (FB-MDP) illustrated in Figure 1a.

FB-MDPs have wide applications (Section 2.1), including modeling delay / latency in the context of network communications and analyzing computation time of offloading tasks in cloud/edge computing systems (Liu et al., 2019; Wei et al., 2019; Chen et al., 2019b). Moreover, FB-MDPs can be employed to discretize forward-backward stochastic differential equations (SDEs) (see Section E.1 for a detailed account), thereby allowing to solve stochastic optimal control problems (Zhang, 2017; Ji et al., 2020). However, forward-backward dynamics have been marginally addressed in the context of RL and MDPs (Section 2.2). In fact, existing research only formulated a deep learning problem in terms of forward-backward SDEs (Ji et al., 2020) or considered artificial backward trajectories in forward MDPs to increase sample efficiency of RL algorithms (Goyal et al., 2019; Wang et al., 2021). To fill this gap, we introduce the concept of FB-MDPs for multi-objective problems

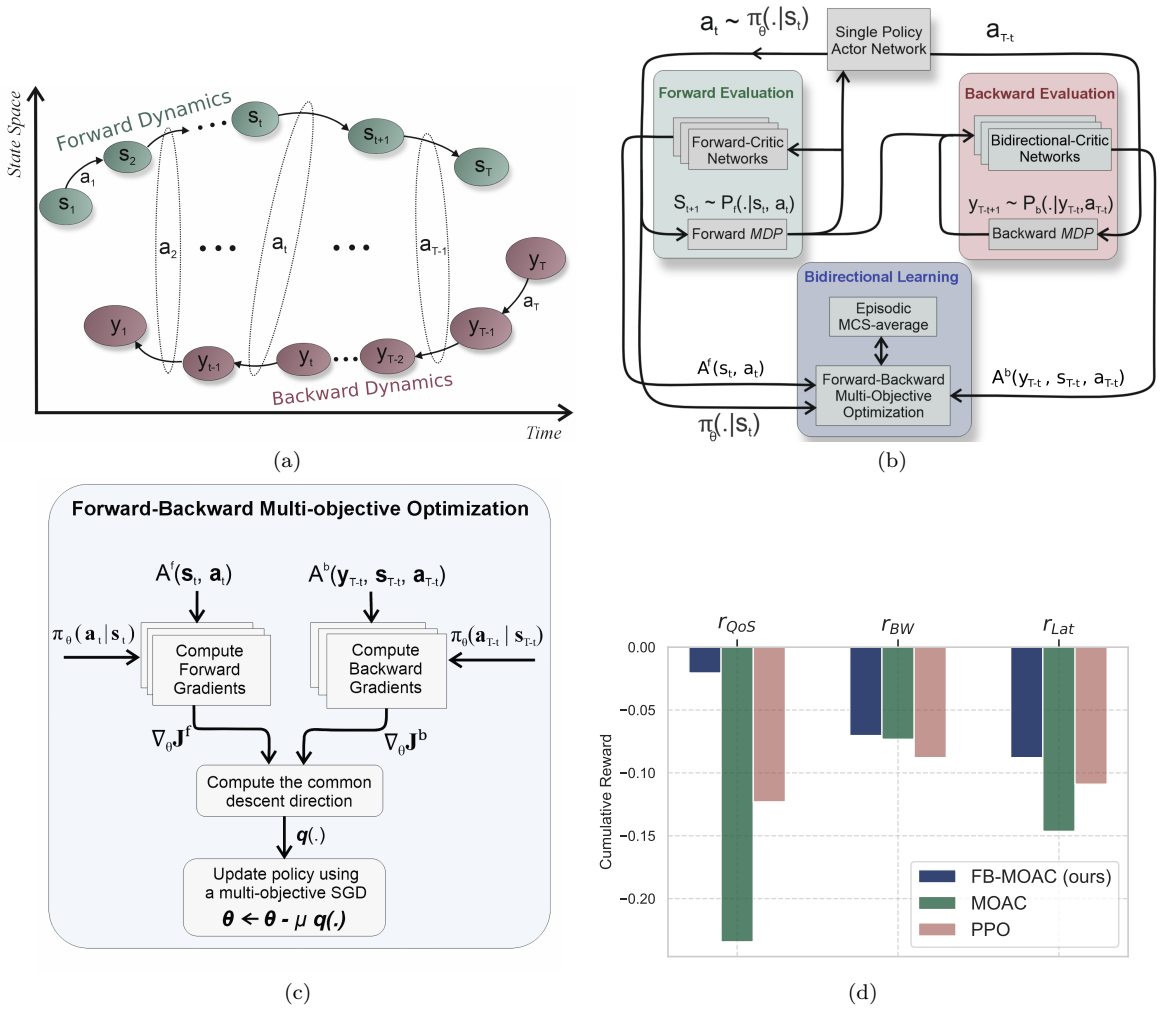

Figure 1: Overview of our approach. (a) A *forward-backward MDP* in which forward states $\{\mathbf{s}_t\}_{t\in\{1,T\}}$ and backward states $\{\mathbf{y}_t\}_{t\in\{1,T\}}$ apply the same actions $\{\mathbf{a}_t\}_{t\in\{1,T\}}$, but with a different ordering in time. (b) The FB-MOAC algorithm comprises three steps: *forward evaluation*, *backward evaluation* and *bidirectional learning*. During the first two steps, the forward and backward dynamics are evaluated and the resulting experiences are buffered. The policy distribution is optimized in the bidirectional learning step based on the experiences of both forward and backward dynamics. For this purpose, it employs a *forward-backward multi-objective optimization* by following an appropriate chronological order. The *episodic MCS-average* add-on boosts the convergence to Pareto-optimal solutions. (c) The multi-objective optimization module of the FB-MOAC algorithm computes: the vector-valued gradients of forward and backward objectives; the descent direction $\mathbf{q}(\cdot)$ to ensure that all rewards increase simultaneously; and finally the parameters of the actor network based on $\mathbf{q}(\cdot)$. (d) Cumulative reward of our approach (FB-MOAC) compared to the widely-used PPO and to MOAC (our multi-objective extension of A2C) in the *edge caching* use case for different metrics (see Section 5.2 for a detailed account). FB-MOAC performs better than the other algorithms in terms of the overall reward.

entailing both forward and backward rewards, and develop an RL algorithm specifically suited to them. In detail, this work establishes the following contributions.

- We introduce the class of *multi-objective FB-MDPs* to express sequential multi-task problems with both forward and backward dynamics, whose rewards are coupled within the action space. We show that these MDPs **cannot** be expressed as a standard MDP, and we consequently develop a novel theoretical framework to characterize their optimal solutions (Section 3).

- We devise a multi-objective RL algorithm, called *Forward-Backward Multi-Objective Actor-Critic* (FB-MOAC), the first of its kind, which employs a step-wise forward-backward mechanism to obtain Pareto-optimal solutions in a preference-insensitive manner. We further provide a rigorous analysis of FB-MOAC, showing that it reaches convergence with a rate of $\mathcal{O}(1/\sqrt{K})$, where K is the number of policy updates (Section 4).
- We conduct a comprehensive evaluation by considering diverse use cases expressed as FB-MDPs in the context of mathematical finance, mobile resource management, and edge computing. The results show that FB-MOAC is effective, whereas standard RL algorithms fail to effectively address these problems (Section 5).

Notation: we use lower-case a for scalars, bold-face lower-case $\mathbf{a}$ for vectors, and bold-face uppercase $\mathbf{A}$ for matrices. Moreover, $\mathbf{A}^\top$ is the transpose of $\mathbf{A}$, $\|\mathbf{A}\|$ is the induced matrix norm of $\mathbf{A}$, $\mathbf{I}$ is the identity matrix, $\mathbf{1}$ a vector with all elements equal to one, $\mathbf{0}$ a vector with all elements equal to zero, and $\mathbf{e}_m$ a vector with all elements equal to zero except the m-th element which is equal to one. Finally, $\boldsymbol{a} = [a_1, \ldots, a_n]^\top$ are the components of a n-dimensional column vector $\boldsymbol{a}$, $|S|$ is the cardinality of the set S, and $[\,\cdot\,]$ indicates the components of row vectors.

2 Background

This section first introduces a few motivating examples of FB-MDPs and then reviews the most relevant works in the existing literature.

2.1 Motivating Examples

Network Content Delivery

Let us consider a scenario in which a content provider (e.g., in a video streaming service) serves users by transmitting N content items with different popularity $\{p_n\}_{n=1}^N$ over a lossy network. Transmissions take place in time slots indexed by t, and the delivery of content n fails with the error probability $e_n(t)$. Upon failure, user requests are re-transmitted until successful delivery. The request probability of content n clearly depends on the success rate of previous requests and the error probability $e_n(t)$. Therefore, it establishes a controlled *forward dynamics* as the content provider affects $e_n(t)$. Now, the average latency $l_n(t)$ experienced by a typical user to successfully receive file n is obtained by: $l_n(t) = d(t)\,(1 - e_n(t)) + (\tau(t) + l_n(t+1))\,e_n(t)$, where: $d(t)$ is the transmission delay between the content provider and he user; and $\tau(t)$ is the duration of time slot t. This equation is obtained by the law of total expectation and exhibits a controlled *backward dynamics* with $l_n(t)$ as a backward state. As a consequence, minimizing the overall latency $\sum_{n=1}^N p_n(t) l_n(t)$ in this context makes the problem an FB-MDP. Now, since a backward MDP cannot be converted to a standard forward MDP (see Theorem 3.6), existing RL algorithms cannot be applied. This is only one instance of network problems that can be modeled as a FB-MDP: Section 5 presents two use cases, one on edge caching in wireless networks and another on computation offloading.

Problems Described by Stochastic Differential Equations

SDEs exhibiting anti-causal dynamics have several applications in the context of differential games (Hamadene & Lepeltier, 1995), diffusion models (Yang et al., 2023), and mathematical finance (Ji et al., 2022a). In particular, problems involving FB-SDEs represent a significant portion of the ongoing research in the field of stochastic control theory (Yong, 2023). Among them, one example is given by an investment-consumption scenario in mathematical finance. Consider a financial market with a single risky asset whose price follows a stochastic process. A trader can invest in this risky asset or engage in risk-free borrowing / lending. The trader's total wealth, $Y(t)$, evolves based on their investment in the asset and the risk-free rate. Now, consider a payoff at a future time T, which depends on the asset's price. The goal is to determine the minimal initial Y_0, required to replicate this payoff. The investment strategy guaranteeing that the final wealth matches the option's payoff is characterized by a backward dynamics (Ji et al., 2022a). In such a context, Section 5.1

presents a use case related to mathematical finance, based on a general method to transform an FB-SDE into a FB-MDP (see Section E.1 for more details).

2.2 Related Work

Forward-Backward MDPs. Our work has some similarity with prior research on RL algorithms (Edwards et al., 2018; Goyal et al., 2019; Wang et al., 2021; Archibald et al., 2023). These studies hypothesize that creating a virtual backward trajectory in relation to a forward MDP enhances the sample-efficiency of RL algorithms. Specifically, they employ the generated backward trajectories to augment the training dataset for learning forward MDP problems. Edwards et al. (2018) train a backwards dynamics to explore in a reverse direction from known goal states. The derived backward paths are then used to augment the replay buffer and contribute to the learning procedure of considered RL algorithm. Similarly, Goyal et al. (2019) learn an artificial backward model – called backtracking model – from the experiences of an agent interacting with the original forward dynamics. The backtracking model then enriches the training dataset by alternative trajectories leading a high value state. Lai et al. (2020); Wang et al. (2021) introduce learnable backward dynamics together with a novel reverse policy to generate paths towards the target states. In particular, they provide informed data augmentation for the training dataset by backpropagating through reverse paths. Our reference model is characterized based on both backward and forward rewards, in contrast with the works described above, wherein backward dynamics are artificially constructed based on a forward MDP. These rewards correspond to actual controlled backward and forward dynamics jointly competing within the action space in both directions of time. Consequently, our investigation is centered around a class of FB-MDPs of multi-task problems with conflicting forward and backward rewards.

Multi-objective RL Algorithms. The majority of Multi-Objective Reinforcement Learning (MO-RL) algorithms has primarily been designed for discrete environments. Mossalam et al. (2016) introduce a MO-RL algorithm that combines deep Q-learning and optimistic linear support learning. Their approach take into account a scalarized vector and potential optima to formulate a convex combination of all objectives. However, they require searching over all potential scalarizing vectors as an a priori knowledge on the importance of distinct objectives is not available. Yang et al. (2019) utilize a multi-objective Q-learning together with a single-agent framework to acquire a preference-related adjustment that can be generalized across different preferences. Such an approach is computationally efficient, however, it often suffers from sample inefficiency and results in a sub-optimal policy. MO-RL algorithms have been specifically developed for continuous environments as well. Zhan & Cao (2019) establish reward-specific state-value functions based on a correlation matrix to obtain the relative importance of objectives with respect to each other. However, their approach requires to adjust the weight of such a matrix to determine an appropriate inter-objective relationship. Abdolmaleki et al. (2020) devise a MO-RL approach according to the *maximum a posteriori policy optimization* algorithm. They learn objective-specific policy distributions to identify Pareto-optimal solutions in a scale-independent manner. However, objective-specific coefficients must be adjusted to control the impact on the policy update. In contrast, we propose a MO-RL algorithm for the continuous-valued FB-MDPs, termed as FB-MOAC, without considering any initial preferences for the different objectives. Different from previous works (Abdolmaleki et al., 2020; Zhan & Cao, 2019; Chen et al., 2019a), we devise a *single-policy approach* to simplify the algorithm and avoids the need for an initial assumption on the reward preference. Moreover, a comprehensive analysis has been conducted to ensure the convergence of FB-MOAC to Pareto-front solutions at a certain rate. A remarkable result of this convergence analysis is the ability of FB-MOAC to monotonically increase all expected objectives for any reward preference, thereby making the algorithm scale-insensitive.

Convergence Analysis of RL algorithms. A few recent works (Qiu et al., 2021; Xu et al., 2020; Fu et al., 2021; Yang et al., 2018; Khodadadian et al., 2022) have explored the characterization of stochastic policy RL algorithms, such as Actor-Critic (AC) and Policy Gradient (Sutton & Barto, 2018). Qiu et al. (2021) conduct a rigorous convergence analysis on the AC algorithm. Notably, their analysis is limited to a linear representation of the state-value function. Xu et al. (2020) provide a comprehensive characterization of the convergence rate and sample complexity of the Natural Actor-Critic (NAC) algorithm (Peters & Schaal, 2008). Their analysis requires that the considered MDP is ergodic. Fu et al. (2021) analyze the convergence of the AC algorithm under the assumption that the considered family of Neural Networks (NNs) are closed

under the Bellman operator. Lastly, Khodadadian et al. (2022) perform a meticulous convergence analysis of the Natural Policy Gradient algorithm (Kakade, 2002). However, their investigation assumes that the initialization value of the state-value function is sufficiently close to the optimal value function. All the aforementioned works address the convergence of stochastic policies of single-objective RL algorithms for forward MDP problems. In contrast, this work targets multi-task problems involving a FB-MDP. We carry out a rigorous convergence analysis as a solid foundation to characterize multi-objective and forward-backward RL algorithms in such a context.

Applications of RL to Network Systems. RL algorithms have also been applied to network systems, particularly, to design dynamic caching and offloading policies (Zhang et al., 2021; Chen et al., 2021; Amidzadeh et al., 2021; Jiang et al., 2022; Chen et al., 2022; Zhou et al., 2023). Chen et al. (2021) devise a multi-agent reinforcement learning for ultra-dense networks, whereas Zhang et al. (2021) employ a deep RL algorithm to jointly optimize resource allocation and caching for Internet-of-Things scenarios. Amidzadeh et al. (2021) leverage a deep RL-based approach to develop an optimal cache policy for multicast-enabled cellular networks. Moreover, Jiang et al. (2022) develop an actor-critic RL algorithm for proactive caching in mobile edge networks. Finally, Chen et al. (2022) and Zhou et al. (2023) employ deep RL for joint caching and offloading problems in edge computing networks. All the works mentioned above only consider forward dynamics, whereas this work entails a more complex characterization that allows to obtain an optimal solution (see Section 5 for a detailed account).

3 Multi-Objective FB-MDPs

This section briefly describes multi-objective optimization and its associated Pareto-optimality as a basis to formally define FB-MDPs. The section concludes by characterizing the optimal solution of a multi-objective FB-MDP problem.

3.1 Pareto Optimality

Consider the following multi-objective optimization problem:

$$\mathrm{Q}_1: \qquad \min_{\boldsymbol{x}\in\mathcal{X}} \quad \big[f_1(\boldsymbol{x}),\ldots,f_r(\boldsymbol{x})\big],$$

where $f_j:\mathbb{R}^N\to\mathbb{R}$, $\mathcal{X}$ is the feasible set and r the number of objectives.

Definition 3.1. We say that $\mathbf{y}\in\mathcal{X}$ Pareto-dominates $\mathbf{x}\in\mathcal{X}$, if $f_i(\boldsymbol{y})\le f_i(\boldsymbol{x})$ for all $i\in\{1,\ldots,r\}$ and there exists $j\in\{1,\ldots,r\}$ such that $f_j(\boldsymbol{y})<f_j(\boldsymbol{x})$.

Definition 3.2. $\boldsymbol{x}^*\in\mathcal{X}$ is called a Pareto-optimal solution of Q_1, if there is no other solution $\boldsymbol{y}\in\mathcal{X}$ that dominates $\boldsymbol{x}^*$. Accordingly, $\big[f_1(\boldsymbol{x}^*),\ldots,f_r(\boldsymbol{x}^*)\big]$ is called a Pareto-optimal vector, and $\min_{\boldsymbol{x}\in\mathcal{X}} \ \big[f_1(\boldsymbol{x}),\ldots,f_r(\boldsymbol{x})\big]$ indicates to the set of Pareto-optimal solutions.

The following lemma (Schäffler et al., 2002; Ma et al., 2020) is instrumental to jointly minimize all objectives of Q_1.

Lemma 3.3. *Consider a vector-valued multivariate function $\boldsymbol{f}=[f_1,\ldots,f_r]$, $f_j:\mathbb{R}^n\to\mathbb{R}$ for $j\in\{1,\ldots,r\}$. Let $\boldsymbol{q}(\cdot)=\sum_{j=1}^r\alpha_j^*\nabla f_j(\cdot)$, then $-\boldsymbol{q}(\cdot)$ is a descent direction for all functions $\{f_j(\cdot)\}_1^r$, where $\{\alpha_j^*\}_1^r$ are the solutions of the following optimization problem:*

$$Q_2: \qquad \min_{\{\alpha_j\}_{j=1}^r} \Big\|\sum_{j=1}^r\alpha_j\nabla f_j(\cdot)\Big\|^2, \qquad \text{s.t.} \quad \sum_{j=1}^r\alpha_j=1, \quad \alpha_j\ge 0, \quad j\in\{1,\ldots,r\}.$$

Remark 3.4. The lemma above can be leveraged to develop a multi-objective gradient descent algorithm. To jointly decrease different objectives, it suffices to optimize $\boldsymbol{\alpha}=[\{\alpha_j\}_{j=1}^r]$ by using the quadratic program Q_2 and obtain $\mathbf{q}(\cdot)$, which is *nonlinear* as $\boldsymbol{\alpha}$ itself depends on $\{\nabla f_j(\cdot)\}_j$.

Accordingly, the optimal solution of problem Q_2 can be obtained as follows.

Corollary 3.5. *If $\nabla \boldsymbol{f}(\cdot)^\top \nabla \boldsymbol{f}(\cdot)$ is invertible and all $\alpha_j \geq 0$, the solution of Q_2 is given by:*

$$\boldsymbol{\alpha}^* = \left(\mathbf{1}_r^\top \left(\nabla \boldsymbol{f}(\cdot)^\top \nabla \boldsymbol{f}(\cdot)\right)^{-1} \mathbf{1}_r\right)^{-1} \left(\nabla \boldsymbol{f}(\cdot)^\top \nabla \boldsymbol{f}(\cdot)\right)^{-1} \mathbf{1}_r, \tag{1}$$

where $\nabla \boldsymbol{f}(\cdot)$ is an $n \times r$ matrix with $\nabla \boldsymbol{f}(\cdot) = \big[\nabla f_1, \ldots, \nabla f_r\big](\cdot)$. For the case $\alpha_j < 0$ for $j \in \mathcal{S}_0 \subset \{1, \ldots, r\}$, we set $\nabla \boldsymbol{f}(\cdot) = [\nabla f_k(\cdot)]_{k \in \{1,\ldots,r\} \setminus \mathcal{S}_0}$.

3.2 Forward-Backward Markov Decision Processes

We introduce a class of *multi-objective FB-MDPs*, expressed by a tuple $\big(\mathcal{S}, \mathcal{Y}, \mathcal{A}, P_f(\cdot), P_b(\cdot), \boldsymbol{r}^f(\cdot), \boldsymbol{r}^b(\cdot)\big)$, where: $\mathcal{S}$ and $\mathcal{Y}$ are the forward and backward state-spaces, respectively; $\mathcal{A}$ is the action space; $P_f \colon \mathcal{S} \times \mathcal{A} \times \mathcal{S} \to [0, 1]$ is the forward transition probability, which describes the forward dynamics; $P_b \colon \mathcal{Y} \times \mathcal{A} \times \mathcal{Y} \to [0, 1]$ is the backward transition probability, which expresses the backward dynamics; and $\boldsymbol{r}^f : \mathcal{S} \times \mathcal{A} \to \mathbb{R}^{|S_f|}$ finally, $\boldsymbol{r}^b : \mathcal{Y} \times \mathcal{A} \to \mathbb{R}^{|S_b|}$ are the forward and backward reward functions, respectively, where S_f and S_b are the sets of indices of the forward and backward rewards. The forward transition probability determines the next forward state of the system $\mathbf{s}_{t+1} \sim P_f(\cdot|\mathbf{s}_t, \mathbf{a}_t)$ starting from $\mathbf{s}_t \in \mathcal{S}$ and performing the action $\mathbf{a}_t \in \mathcal{A}$. Moreover, in an anti-causal way, the previous backward state of the system follows $\mathbf{y}_{t-1} \sim P_b(\cdot|\mathbf{y}_t, \mathbf{a}_t)$ from $\mathbf{y}_t \in \mathcal{Y}$ and performing the action $\mathbf{a}_t \in \mathcal{A}$. The initial forward state $\mathbf{s}_1$ and final backward state $\mathbf{y}_T$ are assumed to be known. Figure 1a on page 2 illustrates a FB-MDP.

Assumption. This work constrains the definition of FB-MDPs to the case where the forward (backward) dynamics does not depend on the backward (forward) state.

Remark 3.6 (**FB-MDPs cannot be expressed as standard MDPs**)**.** The backward dynamics **cannot** be represented based on a standard forward system *in presence of a forward dynamics*. We can consider the transformations $\mathbf{z}_{T-t} := \mathbf{y}_t$ and $t' := T - t$ to convert the backward MDP with transition probability $\mathbf{y}_{t-1} \sim P_b(\cdot|\mathbf{y}_t, \mathbf{a}_t)$ into a forward one. Consequently, we get a forward MDP over $\mathbf{z}_{t'}$ with transition probability $\mathbf{z}_{t'+1} \sim P_b(\cdot|\mathbf{z}_{t'}, \mathbf{a}_{T-t'})$. However, this is a **non-standard** MDP as state z_t becomes a function of actions that are scheduled for future time steps $\mathbf{a}_{T-t}$. Specifically, the state relies on future actions that are not available when progressing forward in time. This violation of the conventional causal structure prevents the use of standard RL algorithms.

The aim of a FB-MDP problem is thus to optimize the following discounted multi-objective cumulative reward from the Pareto-optimality perspective:

$$\max_{\{\mathbf{a}_t \in \mathcal{A}\}_{t \in \{1,T\}}} \mathbb{E}\left\{\sum_{t=1}^{T} \gamma^{t-1} \left[\boldsymbol{r}^f(\mathbf{s}_t, \mathbf{a}_t),\ \boldsymbol{r}^b(\mathbf{y}_{T-t+1}, \mathbf{a}_{T-t+1})\right]\right\}, \tag{2}$$

In Equation (2), $T \in \mathbb{N}$ is the finite horizon of the optimization, $\gamma \in [0, 1]$ the discount factor, and the expectation refers to the different realizations of the forward-backward trajectory.

Remark 3.6 highlights that solving a FB-MDP problem of the type in Equation (2) requires developing novel theoretical foundations. To do so, we build on the following observation and the resulting optimal solutions.

Remark 3.7. Both the forward and backward dynamics of a FB-MDP problem can be accurately learned through a $\boldsymbol{\theta}$-parametric stochastic policy $\mathbf{a}_t \sim \pi_{\boldsymbol{\theta}}(\cdot|\mathbf{s}_t)$, whereas employing the policy $\mathbf{a}_t \sim \pi_{\boldsymbol{\theta}}(\cdot|\mathbf{s}_t, \mathbf{y}_t)$ is unfeasible due to the anti-causal nature of the backward dynamics. Therefore, we need to optimize the policy $\pi_{\boldsymbol{\theta}}(\cdot|\mathbf{s}_t)$ based on the trajectories of both forward and backward dynamics.

The following section delves into this process.

3.3 Characterizing an Optimal Solution

We now analyze Remark 3.7 and provide a theoretical framework to characterize the optimal solution of a multi-objective FB-MDP problem. Accordingly, the probability of a forward-backward trajectory $\boldsymbol{\tau}$ is

determined by:

$$\begin{aligned}\mathrm{P}_{\boldsymbol{\theta}}(\boldsymbol{\tau}) :&= \mathbb{P}(\mathbf{s}_1, \mathbf{a}_1, \ldots, \mathbf{s}_T, \mathbf{a}_T, \mathbf{y}_T, \ldots, \mathbf{y}_1) \\ &= \mathbb{P}(\mathbf{s}_1) \prod_{t=1}^{T-1} P_f(\mathbf{s}_{t+1}|\mathbf{s}_t, \mathbf{a}_t) \prod_{t=1}^{T-1} \pi_{\boldsymbol{\theta}}(\mathbf{a}_t|\mathbf{s}_t) \prod_{t=1}^{T-1} P_b(\mathbf{y}_{T-t}|\mathbf{y}_{T-t+1}, \mathbf{a}_{T-t+1})\mathbb{P}(\mathbf{y}_T). \end{aligned} \tag{3}$$

The problem in Equation (2) is then reformulated as the following *policy distribution optimization*:

$$\begin{aligned}\mathrm{O}_2 : \qquad \max_{\boldsymbol{\theta}} \ & \mathbb{E}_{\tau\sim \mathrm{P}_{\boldsymbol{\theta}}(\boldsymbol{\tau})}\Big\{ \sum_{t=1}^{T} \gamma^{t-1} \Big[\boldsymbol{r}^f(\mathbf{s}_t, \mathbf{a}_t),\, \boldsymbol{r}^b(\mathbf{y}_{T-t+1}, \mathbf{a}_{T-t+1}) \Big] \ \Big| \ \boldsymbol{\theta} \Big\} \\ & \text{s.t.} \ \Big\{ \mathbf{s}_{t+1} \sim P_f(\cdot|\mathbf{s}_t, \mathbf{a}_t), \qquad \mathbf{y}_{t-1} \sim P_b(\cdot|\mathbf{y}_t, \mathbf{a}_t), \qquad \mathbf{a}_t \sim \pi_{\boldsymbol{\theta}}(\cdot|\mathbf{s}_t) \Big\}. \end{aligned} \tag{4}$$

The multivariate objective of O_2 can thus be expressed as:

$$\mathbf{J}(\boldsymbol{\theta}) := \Big[\underbrace{\mathbb{E}_{\tau\sim \mathrm{P}_{\boldsymbol{\theta}}(\boldsymbol{\tau})} \sum_{k=1}^{T} \gamma^{k-1} \boldsymbol{r}^f(\mathbf{s}_k, \mathbf{a}_k)}_{\mathbf{J}^f(\boldsymbol{\theta})}, \quad \underbrace{\mathbb{E}_{\tau\sim \mathrm{P}_{\boldsymbol{\theta}}(\boldsymbol{\tau})} \sum_{k=1}^{T} \gamma^{k-1} \boldsymbol{r}^b(\mathbf{y}_{T-k+1}, \mathbf{a}_{T-k+1})}_{\mathbf{J}^b(\boldsymbol{\theta})} \Big].$$

To Pareto optimize $\mathbf{J}(\boldsymbol{\theta})$, we need to first compute its component-wise gradient with respect to $\boldsymbol{\theta}$, i.e., $\nabla_{\boldsymbol{\theta}} \mathbf{J}(\boldsymbol{\theta}) = \frac{\partial \mathbf{J}(\boldsymbol{\theta})}{\partial \mathrm{P}_{\boldsymbol{\theta}}(\boldsymbol{\tau})} \frac{\partial \mathrm{P}_{\boldsymbol{\theta}}(\boldsymbol{\tau})}{\partial \boldsymbol{\theta}}$. For the forward cumulative rewards $\mathbf{J}^f(\boldsymbol{\theta})$, we have (Grondman et al., 2012):

$$\nabla_{\boldsymbol{\theta}} \mathbf{J}^f(\boldsymbol{\theta}) = \mathbb{E}\Big\{ \sum_{k=1}^{T} \nabla_{\boldsymbol{\theta}} \log \pi_{\boldsymbol{\theta}}(\mathbf{a}_k|\mathbf{s}_k) \mathbf{A}^f(\mathbf{s}_k, \mathbf{a}_k) \ \Big| \ \boldsymbol{\theta} \Big\}, \tag{5}$$

where: $\mathbf{A}^f : \mathcal{S} \times \mathcal{A} \to \mathbb{R}^{|S_f|}$, $\mathbf{A}^f(\mathbf{s}_k, \mathbf{a}_k) := \boldsymbol{r}^f(\mathbf{s}_k, \mathbf{a}_k) + \gamma V^f(\mathbf{s}_{k+1}) - V^f(\mathbf{s}_k)$ is the forward advantage multivariate function; and $V^f : \mathcal{S} \to \mathbb{R}^{|S_f|}$, $V^f(\mathbf{s}_k) := \mathbb{E}\Big\{ \sum_{k'=k}^{T} \gamma^{k'-k} \boldsymbol{r}^f(\mathbf{s}_{k'}, \mathbf{a}_{k'}) \big| \mathbf{s}_k \Big\}$ is the forward state-value multivariate function. We finally obtain the following lemma to characterize the optimal backward trajectories and the Pareto-optimal solutions of FB-MDP problem O_2.

Lemma 3.8. *For the backward cumulative reward $\boldsymbol{J}^b(\boldsymbol{\theta})$, it is:*

$$\nabla_{\boldsymbol{\theta}} \boldsymbol{J}^b(\boldsymbol{\theta}) = \mathbb{E}_{P_{\boldsymbol{\theta}}(\boldsymbol{\tau})}\Big\{ \sum_{k=0}^{T-1} \nabla_{\boldsymbol{\theta}} \log \pi_{\boldsymbol{\theta}}(\boldsymbol{a}_{T-k}|\boldsymbol{s}_{T-k}) \boldsymbol{A}^b(\boldsymbol{y}_{T-k}, \boldsymbol{s}_{T-k}, \boldsymbol{a}_{T-k}) \ \Big| \ \boldsymbol{\theta} \Big\}, \tag{6}$$

where $A^b : \mathcal{Y} \times \mathcal{S} \times \mathcal{A} \to \mathbb{R}^{|S_b|}$ is the bidirectional advantage multivariate function:

$$A^b(\boldsymbol{y}_{T-k}, \boldsymbol{s}_{T-k}, \boldsymbol{a}_{T-k}) := \boldsymbol{r}^b(\boldsymbol{y}_{T-k}, \boldsymbol{a}_{T-k}) + \gamma V^b(\boldsymbol{y}_{T-k-1}, \boldsymbol{s}_{T-k-1}) - V^b(\boldsymbol{y}_{T-k}, \boldsymbol{s}_{T-k}),$$

and $V^b : \mathcal{Y} \times \mathcal{S} \to \mathbb{R}^{|S_b|}$ is the bidirectional state-value multivariate function:

$$V^b(\boldsymbol{y}_{T-k}, \boldsymbol{s}_{T-k}) := \mathbb{E}\Big\{ \sum_{k'=T-k}^{1} \gamma^{T-k'-1} \boldsymbol{r}^b(\boldsymbol{y}_{k'}, \boldsymbol{a}_{k'}) \big| \boldsymbol{y}_{T-k}, \boldsymbol{s}_{T-k} \Big\} = \mathbb{E}\Big\{ \sum_{k'=k}^{T-1} \gamma^{k'-k} \boldsymbol{r}^b(\boldsymbol{y}_{T-k'}, \boldsymbol{a}_{T-k'}) \big| \boldsymbol{y}_{T-k}, \boldsymbol{s}_{T-k} \Big\},$$

which adheres to the backward Bellman's equation:

$$V^b(\boldsymbol{y}_{T-k}, \boldsymbol{s}_{T-k}) \quad = \quad \mathop{\mathbb{E}}_{\substack{\boldsymbol{a}_{T-k} \sim \pi_{\boldsymbol{\theta}}(\cdot|\boldsymbol{s}_{T-k}) \\ \boldsymbol{y}_{T-k-1} \sim P_b(\cdot|\boldsymbol{y}_{T-k}, \boldsymbol{a}_{T-k}) \\ \boldsymbol{s}_{T-k-1} \sim P(\cdot|\boldsymbol{s}_{T-k})}} \Big\{ \boldsymbol{r}^b(\boldsymbol{y}_{T-k}, \boldsymbol{a}_{T-k}) + \gamma V^b(\boldsymbol{y}_{T-k-1}, \boldsymbol{s}_{T-k-1}) \big| \boldsymbol{\theta} \Big\}. \tag{7}$$

For the stationary forward and backward transition probabilities, a Bellman Pareto-optimality equation is given by:

$$\Big[V^{f^*}(\boldsymbol{s}), V^{b^*}(\boldsymbol{y}, \boldsymbol{s}) \Big] \in \max_{\boldsymbol{a}} \left[\mathop{\mathbb{E}}_{s^+ \sim P_f(\cdot|s,\, a)} \Big\{ \boldsymbol{r}^f(\boldsymbol{s}, \boldsymbol{a}) + \gamma V^{f^*}\left(\boldsymbol{s}^+\right) \Big\}, \mathop{\mathbb{E}}_{\substack{y^- \sim P_b(\cdot|y,\, a) \\ s^- \sim P(\cdot|s)}} \Big\{ \boldsymbol{r}^b(\boldsymbol{y}, \boldsymbol{a}) + \gamma V^{b^*}\left(\boldsymbol{y}^-, \boldsymbol{s}^-\right) \Big\} \right], \tag{8}$$

for $(\boldsymbol{s}, \boldsymbol{y}, \boldsymbol{a}) \in \mathcal{S} \times \mathcal{Y} \times \mathcal{A}$, where $\big[V^{f^*}(\boldsymbol{s}), V^{b^*}(\boldsymbol{y}, \boldsymbol{s})\big]$ is a Pareto-optimal vector, $\boldsymbol{s}^+ \in \mathcal{S}$ is the forward state following $\boldsymbol{s}$, and $\boldsymbol{y}^- \in \mathcal{Y}$ is the backward state preceding $\boldsymbol{y}$.

Proof. Please refer to Appendix A. □

Remark 3.9. The formulation of this lemma differs from its counterpart for forward MDPs. Specifically, the bidirectional state-value $V^b(\mathbf{y}_{T-k}, \mathbf{s}_{T-k})$ is defined in Equation (7) *so as to* have a backward Bellman's equation. Note that Equation (7) exhibits a forward dynamics with a dependency on the policy distribution that itself relies on the forward state rather than the backward state. Moreover, the *Bellman's Pareto-optimality* equation [i.e., Equation (8)] characterizes an optimal solution for FB-MDPs, which notably exhibits a bidirectional optimality dynamics, due to presence of $\mathbf{s}^-$ and $\mathbf{s}^+$ on RHS. This requires that both dynamics should be jointly and *simultaneously* considered to obtain an optimal policy. We leverage these findings in devising our algorithm next.

4 Forward-Backward Multi-Objective RL

We now build on the results in the previous section to develop an RL algorithm for multi-objective FB-MDP problems. Specifically, we devise a *Forward-Backward Step-Wise* (FB-SW) mechanism according to Theorem 3.7 and Theorem 3.8. The mechanism comprises of three steps: *forward evaluation*, in which the forward dynamics is evaluated by generating actions using the policy $\mathbf{a}_t \sim \pi_{\boldsymbol{\theta}}(\cdot|\mathbf{s}_t)$; *backward evaluation*, in which the backward dynamics is evaluated in a time-reversed way by leveraging the actions generated in the previous step; and *bidirectional learning*, leveraging a multi-objective optimization mechanism *with a suitable chronological order* to optimize the policy $\pi_{\boldsymbol{\theta}}(\cdot|\mathbf{s}_t)$ based on the experiences obtained from both the forward and backward dynamics. Figures 1b and 1c on page 2 outline the resulting algorithm.

4.1 The Forward-Backward Algorithm

According to Equations (5) and (6), the gradient of $\mathbf{J}(\boldsymbol{\theta})$ depends on the policy distribution $\pi_{\boldsymbol{\theta}}(\cdot|\cdot)$ in addition to the state-value functions $V^f(\cdot)$ and $V^b(\cdot,\cdot)$. For the policy distribution $\pi_{\boldsymbol{\theta}}(\cdot|\cdot)$, we consider an *actor agent* represented by a $\boldsymbol{\theta}$-parametric neural network (NN). For the forward state-value function $V^f(\cdot)$, we set a *forward-critic network* represented by a $\boldsymbol{\phi}$-parametric NN, denoted by $V^f_{\boldsymbol{\phi}}(\cdot)$. Moreover, we use a *backward-critic network* with a $\boldsymbol{\psi}$-parametric NN for the bidirectional state-value function, indicated by $V^b_{\boldsymbol{\psi}}(\cdot,\cdot)$. We must now align the evaluation and update procedures for the actor and critic networks with the FB-SW mechanism. In this regard, $\pi_{\boldsymbol{\theta}}(\cdot|\cdot)$ and $V^f_{\boldsymbol{\phi}}(\cdot)$ are evaluated during the forward-evaluation step of the FB-SW mechanism, $V^b_{\boldsymbol{\psi}}(\cdot,\cdot)$ is evaluated during the backward-evaluation step, then their values are employed to compute $\nabla_{\boldsymbol{\theta}}\mathbf{J}(\boldsymbol{\theta})$ and update $\pi_{\boldsymbol{\theta}}(\cdot|\cdot)$ during the forward-backward optimization step.

The update mechanism of actor policy $\pi_{\boldsymbol{\theta}}(\cdot|\cdot)$ depends on the forward and bidirectional state-value functions, i.e., $V^f_{\boldsymbol{\phi}}(\cdot)$ and $V^b_{\boldsymbol{\psi}}(\cdot,\cdot)$. As a consequence, we need to set some losses to also update these state-value functions. In line with Bellman's equation $V^f(\mathbf{s}_k) = \mathbb{E}_{\mathbf{s}_{k+1},\mathbf{a}_k|\mathbf{s}_k}\{\boldsymbol{r}^f(\mathbf{s}_k,\mathbf{a}_k) + \gamma V^f(\mathbf{s}_{k+1})\}$ and Temporal Difference (TD)-learning (Grondman et al., 2012), the following *forward-critic losses* are considered to update $\boldsymbol{\phi}$:

$$\sum_{k=1}^{T} A^f_{\boldsymbol{\phi},i}(\mathbf{s}_k,\mathbf{a}_k)^2, \quad \text{for} \;\; i \in S_f, \tag{9}$$

where $A^f_{\boldsymbol{\phi},i}(\mathbf{s}_k,\mathbf{a}_k) = V^f_{\boldsymbol{\phi},i}(\mathbf{s}_k) - r^f_i(\mathbf{s}_k,\mathbf{a}_k) - \gamma V^f_{\boldsymbol{\phi},i}(\mathbf{s}_{k+1})$ are parametric representations for the so-called forward advantage functions. Conversely, we set the following *backward-critic losses* to update the parameter $\boldsymbol{\psi}$ based on the derived backward Bellman's equation [i.e., Equation (7)]:

$$\sum_{k=0}^{T-1} A^b_{\boldsymbol{\psi},i}(\mathbf{y}_{T-k},\mathbf{s}_{T-k},\mathbf{a}_{T-k})^2, \quad \text{for} \;\; i \in S_b, \tag{10}$$

where $A^b_{\boldsymbol{\psi},i}(\mathbf{y}_{T-k},\mathbf{s}_{T-k},\mathbf{a}_{T-k}) = V^b_{\boldsymbol{\psi},i}(\mathbf{y}_{T-k},\mathbf{s}_{T-k}) - r^b_i(\mathbf{y}_{T-k},\mathbf{a}_{T-k}) - \gamma V^b_{\boldsymbol{\psi},i}(\mathbf{y}_{T-k-1},\mathbf{s}_{T-k-1})$ are the parametric bidirectional advantage functions.

Equations (5) and (6) indicate multiple losses for optimizing the actor and Equations (9) and (10) show multiple losses for optimizing the forward / bidirectional critic networks. A straightforward approach to

carry out multi-objective optimization involves using the scalarization technique, namely, obtaining a single-objective loss through a preference function (or scales) for different losses. However, Pareto solutions cannot be necessarily obtained via this method (Kirlik & Sayın, 2014). As a consequence, tuning the scalarization settings might require a trial-and-error approach, which is sensitive to the selected setup. Instead, we use a scale-insensitive multi-objective optimization method (Schäffler et al., 2002) to devise a forward-backward RL algorithm. Accordingly, we employ Lemma 3.3 to formulate forward / bidirectional critic networks and a multi-objective actor agent shared between the forward and bidirectional critics.

4.1.1 Forward / Bidirectional Critic Networks

Equation (9) [Equation (10)] provides multiple losses for the forward (backward) critic network. By recalling Lemma 3.3, we formulate the *multi-objective* loss $K^f(\boldsymbol{\phi})$ $[K^b(\boldsymbol{\psi})]$ by using the coefficients $\boldsymbol{\beta_f}$ $(\boldsymbol{\beta_b})$, so that a common descent direction is formulated for all forward (backward) losses. Accordingly, we have:

$$K^f(\boldsymbol{\phi}) = \sum_{j\in S_f} \beta^*_{f,j} \sum_{k=1}^{T} A^f_{\boldsymbol{\phi},j}(\mathbf{s}_k, \mathbf{a}_k)^2, \qquad K^b(\boldsymbol{\psi}) = \sum_{j\in S_b} \beta^*_{b,j} \sum_{k=0}^{T-1} A^b_{\boldsymbol{\psi},j}(\mathbf{y}_{T-k}, \mathbf{s}_{T-k}, \mathbf{a}_{T-k})^2, \tag{11}$$

where $\boldsymbol{\beta}^*_f$ and $\boldsymbol{\beta}^*_b$ are tuned by the following problems (see Q_2 of Lemma 3.3):

$$\boldsymbol{\beta}^*_f = \underset{\substack{\beta_j \geq 0 \\ \sum_{j\in S_f} \beta_j = 1}}{\operatorname{argmin}} \left\| \sum_{j\in S_f} \beta_j \nabla_{\boldsymbol{\phi}} \sum_{k=1}^{T} A^f_{\boldsymbol{\phi},j}(\mathbf{s}_k, \mathbf{a}_k)^2 \right\|^2, \qquad \boldsymbol{\beta}^*_b = \underset{\substack{\beta_j \geq 0 \\ \sum_{j\in S_b} \beta_j = 1}}{\operatorname{argmin}} \left\| \sum_{j\in S_b} \beta_j \nabla_{\boldsymbol{\psi}} \sum_{k=0}^{T-1} A^b_{\boldsymbol{\psi},j}(\mathbf{y}_{T-k}, \mathbf{s}_{T-k}, \mathbf{a}_{T-k})^2 \right\|^2. \tag{12}$$

These critic networks are then updated via TD-learning with the following Stochastic Gradient Descent (SGD) rules (Grondman et al., 2012):

$$\boldsymbol{\phi} \leftarrow \boldsymbol{\phi} - \mu_f \nabla_{\boldsymbol{\phi}} K^f(\boldsymbol{\phi}), \qquad \boldsymbol{\psi} \leftarrow \boldsymbol{\psi} - \mu_b \nabla_{\boldsymbol{\psi}} K^b(\boldsymbol{\psi}), \tag{13}$$

where μ_f and μ_b are the learning rates of the forward and bidirectional critic networks, respectively.

4.1.2 Actor Agent

We follow the same strategy as in the previous section to devise a single-policy multi-objective actor agent shared between the forward and backward processes. The following forward and backward gradients follow from Equations (5) and (6) and are given by:

$$\begin{aligned} \nabla_{\boldsymbol{\theta}} \hat{J}^f_i(\boldsymbol{\theta}, \boldsymbol{\phi}) &= -\sum_{k=1}^{T} \nabla_{\boldsymbol{\theta}} \log \pi_{\boldsymbol{\theta}}(\mathbf{a}_k|\mathbf{s}_k) A^f_{\boldsymbol{\phi},i}(\mathbf{s}_k, \mathbf{a}_k), \\ \nabla_{\boldsymbol{\theta}} \hat{J}^b_j(\boldsymbol{\theta}, \boldsymbol{\psi}) &= -\sum_{k=0}^{T-1} \nabla_{\boldsymbol{\theta}} \log \pi_{\boldsymbol{\theta}}(\mathbf{a}_{T-k}|\mathbf{s}_{T-k}) A^b_{\boldsymbol{\psi},j}(\mathbf{y}_{T-k}, \mathbf{s}_{T-k}, \mathbf{a}_{T-k}) \end{aligned} \tag{14}$$

for $i \in S_f$ and $j \in S_b$. We then employ Lemma 3.3 to provide a simultaneous descent direction for all forward / backward rewards. Hence, the multi-objective actor agent is updated by the following multi-objective SGD:

$$\boldsymbol{\theta} \leftarrow \boldsymbol{\theta} - \mu\big(\sum_{j\in S_f} \beta_{\mathrm{act,j}} \nabla_{\boldsymbol{\theta}} \hat{J}^f_j(\boldsymbol{\theta}, \boldsymbol{\phi}) + \sum_{j\in S_b} \beta_{\mathrm{act,j}} \nabla_{\boldsymbol{\theta}} \hat{J}^b_j(\boldsymbol{\theta}, \boldsymbol{\psi}) \big), \tag{15}$$

where μ is the learning rate of actor agent, and

$$\boldsymbol{\beta}_{\mathrm{act}} = \underset{\{\beta_j\}_j}{\operatorname{argmin}} \left\| \sum_{j\in S_f} \beta_j \nabla_{\boldsymbol{\theta}} \bar{J}^f_j(\boldsymbol{\theta}) + \sum_{j\in S_b} \beta_j \nabla_{\boldsymbol{\theta}} \bar{J}^b_j(\boldsymbol{\theta}) \right\|^2, \tag{16}$$

$$\text{s.t.} \quad \beta_j \geq 0, \qquad \sum_{j\in S_f \cup S_b} \beta_j = 1, \tag{17}$$

with

$$\nabla_{\boldsymbol{\theta}} \bar{J}_i^b(\boldsymbol{\theta}) := -\mathbb{E}_{\boldsymbol{\psi}} \mathbb{E}\left\{ \sum_{k=0}^{T-1} \nabla_{\boldsymbol{\theta}} \log \pi_{\boldsymbol{\theta}}(\mathbf{a}_{T-k}|\mathbf{s}_{T-k}) A^b_{\boldsymbol{\psi},i}(\mathbf{y}_{T-k}, \mathbf{s}_{T-k}, \mathbf{a}_{T-k}) \,\middle|\, \boldsymbol{\theta}, \boldsymbol{\psi} \right\},$$
$$\nabla_{\boldsymbol{\theta}} \bar{J}_j^f(\boldsymbol{\theta}) := -\mathbb{E}_{\boldsymbol{\phi}} \mathbb{E}\left\{ \sum_{k=1}^{T} \nabla_{\boldsymbol{\theta}} \log \pi_{\boldsymbol{\theta}}(\mathbf{a}_k|\mathbf{s}_k) A^f_{\boldsymbol{\phi},j}(\mathbf{s}_k, \mathbf{a}_k) \,\middle|\, \boldsymbol{\theta}, \boldsymbol{\phi} \right\}, \tag{18}$$

for $j \in S_f$ and $i \in S_b$. Note that, as opposed to the critic losses, we theoretically leverage the expected gradient $\nabla_{\boldsymbol{\theta}} \bar{J}_j^f(\boldsymbol{\theta})$ and $\nabla_{\boldsymbol{\theta}} \bar{J}_j^b(\boldsymbol{\theta})$ to optimize $\boldsymbol{\beta}_{\text{act}}$ in Equation (16) [compare with Equation (12)]. This approach interestingly guarantees that all forward and backward cumulative losses – namely, $\{J_j^f(\boldsymbol{\theta})\}_{j\in|S|_f}$ and $\{J_i^b(\boldsymbol{\theta})\}_{i\in|S|_b}$ – monotonically decrease with each iteration. Please refer to Theorem B.1 in the appendix for more details.

To estimate the expected gradients $\nabla_{\boldsymbol{\theta}} \bar{J}_j^f(\boldsymbol{\theta})$ and $\nabla_{\boldsymbol{\theta}} \bar{J}_j^b(\boldsymbol{\theta})$, we employ *Monte Carlo Sampling* (MCS) together with an *exponential moving average*, applied to $\nabla_{\boldsymbol{\theta}} \hat{J}_j^f(\boldsymbol{\theta}, \boldsymbol{\phi})$ and $\nabla_{\boldsymbol{\theta}} \hat{J}_j^b(\boldsymbol{\theta}, \boldsymbol{\psi})$. Specifically, we first implement N_{mcs} distinct backward and forward critic networks with learnable parameters $\{\boldsymbol{\psi}_l\}_{l=1}^{N_{\text{mcs}}}$ and $\{\boldsymbol{\phi}_l\}_{l=1}^{N_{\text{mcs}}}$, respectively, and use the approximations

$$\nabla_{\boldsymbol{\theta}} \bar{J}_j^f(\boldsymbol{\theta}) \approx \frac{1}{N_{\text{MCS}}} \sum_{l=1}^{N_{\text{MCS}}} \mathbb{E}\left\{ \nabla_{\boldsymbol{\theta}} \hat{J}_j^f(\boldsymbol{\theta}, \boldsymbol{\phi}_l) | \boldsymbol{\theta} \right\}, \qquad \nabla_{\boldsymbol{\theta}} \bar{J}_i^b(\boldsymbol{\theta}) \approx \frac{1}{N_{\text{MCS}}} \sum_{l=1}^{N_{\text{MCS}}} \mathbb{E}\left\{ \nabla_{\boldsymbol{\theta}} \hat{J}_i^b(\boldsymbol{\theta}, \boldsymbol{\psi}_l) | \boldsymbol{\theta} \right\}.$$

In addition, we consider different episodes to take an exponential average with a smoothing factor γ_{mov} to estimate $\mathbb{E}\left\{ \nabla_{\boldsymbol{\theta}} \hat{J}_j^f(\boldsymbol{\theta}, \boldsymbol{\phi}_l) | \boldsymbol{\theta} \right\}$ and $\mathbb{E}\left\{ \nabla_{\boldsymbol{\theta}} \hat{J}_i^b(\boldsymbol{\theta}, \boldsymbol{\psi}_l) | \boldsymbol{\theta} \right\}$. We name this approach **episodic MCS-average**.

Figure 1b overviews the proposed Forward-Backward Multi-Objective Actor-Critic (FB-MOAC) algorithm, whereas Algorithm 1 provides its pseudo-code.

4.2 Optimality and Convergence

The episodic MCS-average approach enables us to prove the convergence of FB-MOAC to a Pareto-optimal solution.

Theorem 4.1. *For Lipschitz-smooth losses, FB-MOAC reaches convergence to a locally Pareto-optimal solution with a rate of $\mathcal{O}(1/\sqrt{K})$, where K is the number of policy updates.*

Proof (sketch). It can be shown that the episodic MCS-average approach ensures the forward and backward expected losses $\{J_j^f(\boldsymbol{\theta})\}_{j\in|S_f|}$ and $\{J_i^b(\boldsymbol{\theta})\}_{i\in|S_b|}$ constantly decrease at each iteration based on Corollary 3.5. This fact and the characteristic features of Lipschitz-smooth losses guarantee convergence to a locally non-dominated Pareto-optimal solution with a rate of $\mathcal{O}(1/\sqrt{K})$. Appendix B.2 provides a complete proof.

□

Remark 4.2. The convergence results of Theorem 4.1 are aligned with those of single-optimization algorithms for forward-MDPs (Fu et al., 2021).

Remark 4.3. The computational complexity of FB-MOAC is primarily described by its convergence rate, which is competitive to standard algorithms. However, the episodic MCS-average add-on makes FB-MOAC computationally different from standard algorithms. The convergence of the add-on depends on the number of the critic agents; however, three agents are already enough to reach convergence in practice (see Section 5 for more details). Consequently, the overall complexity of FB-MOAC remains competitive with respect to forward-only RL algorithms.

Remark 4.4. Appendix B.1 proves that FB-MOAC has a faster convergence, with a rate of $\mathcal{O}(1/K)$, when the losses are both strongly convex and Lipschitz-smooth.

Algorithm 1 Pseudo-code of the Forward-Backward Multi-Objective Actor-Critic (FB-MOAC) algorithm.

for *episode* $= 1$ **to** $E_{\max}$ **do**
  Input: Initial forward-backward state $(\mathbf{s}_1, \mathbf{y}_T)$.
    Actor, forward-critic and backward-critic parameters: $\boldsymbol{\theta}$, $\boldsymbol{\phi}$ and $\boldsymbol{\psi}$.
Forward Evaluation:
  for $t = 1$ **to** T **do**
    Select $\mathbf{a}_t \sim \pi_{\boldsymbol{\theta}}(\cdot|\mathbf{s}_t)$, interact with environment.
    Observe forward state $\mathbf{s}_{t+1}$ and forward rewards $\{r_j^f(\mathbf{s}_t, \mathbf{a}_t)\}_{j\in S_f}$.
    Compute $\{A^f_{\boldsymbol{\phi},j}(\mathbf{s}_t, \mathbf{a}_t)\}_{j\in S_f}$ by forward state-value $\{V^f_{\boldsymbol{\phi},j}(\mathbf{s}_t)\}_{j\in S_f}$, Equation (9).
    Compute $\log\big(\pi_{\boldsymbol{\theta}}(\mathbf{a}_t|\mathbf{s}_t)\big)$.
  end for
Backward Evaluation:
  for $t = 1$ **to** T **do**
    Observe backward state $\mathbf{y}_{T-t}$ and backward rewards $\{r_j^b(\mathbf{y}_{T-t}, \mathbf{a}_{T-t})\}_{j\in S_b}$ depending on the drawn action of step *Forward-Evaluation*.
    Compute $\{A^b_{\boldsymbol{\psi},j}(\mathbf{y}_{T-t}, \mathbf{s}_{T-t}, \mathbf{a}_{T-t})\}_{j\in S_b}$ by bidirectional state-value $\{V^b_{\boldsymbol{\psi},j}(\mathbf{y}_{T-t}, \mathbf{s}_{T-t})\}_{j\in S_b}$, Equation (10).
  end for
Forward-Backward Optimization:
  Forward / bidirectional critic Update:
  Obtain $\boldsymbol{\beta}_f^*$ and $\boldsymbol{\beta}_b^*$ by Equation (12).
  Compute multi-objective forward-critic loss $K^f(\boldsymbol{\phi})$ and backward-critic loss $K^b(\boldsymbol{\psi})$.
  Apply the rules:

$$\boldsymbol{\phi} \leftarrow \boldsymbol{\phi} - \mu_f \nabla_{\boldsymbol{\phi}} K^f(\boldsymbol{\phi}), \qquad \boldsymbol{\psi} \leftarrow \boldsymbol{\psi} - \mu_b \nabla_{\boldsymbol{\psi}} K^b(\boldsymbol{\psi}).$$

  Forward-Backward Optimization:
  Obtain $\boldsymbol{\beta}^*$ using Equation (16) and the outcomes of *episodic MCS-average*.
  Compute stochastic forward and backward gradients $\nabla_{\boldsymbol{\theta}} \hat{J}_j^f(\boldsymbol{\theta}, \boldsymbol{\phi})$ and $\nabla_{\boldsymbol{\theta}} \hat{J}_j^b(\boldsymbol{\theta}, \boldsymbol{\psi})$ using Equation (14).
  Apply the SGD rule:

$$\boldsymbol{\theta} \leftarrow \boldsymbol{\theta} - \mu\Big(\sum_{j\in S_f} \beta_{\text{act,j}} \nabla_{\boldsymbol{\theta}} \hat{J}_j^f(\boldsymbol{\theta}, \boldsymbol{\phi}) + \sum_{j\in S_b} \beta_{\text{act,j}} \nabla_{\boldsymbol{\theta}} \hat{J}_j^b(\boldsymbol{\theta}, \boldsymbol{\psi})\Big),$$

end for

4.3 Deriving the Pareto-Front

Our FB-MOAC algorithm is designed as a multi-objective framework where a single-policy agent interacts with **multiple** reward-specific critic networks. Crucially, these critics are updated through a non-linear mechanism with respect to the reward functions, as described by Remark 3.4 in addition to Equations (11) and (13). Hence, we consider the critics for developing a preference policy with respect to different rewards. To systematically explore the Pareto front, we introduce forward and backward preference parameters, $\boldsymbol{\epsilon}^f \in (0,1]^{|S_f|}$, $\boldsymbol{\epsilon}^b \in (0,1]^{|S_b|}$, which are used to re-scale the corresponding advantage functions:

$$\begin{aligned} A_i^f(\mathbf{s}_k, \mathbf{a}_k) &= \epsilon_i^f \; r_i^f(\mathbf{s}_k, \mathbf{a}_k) + \gamma V_i^f(\mathbf{s}_{k+1}) - V_i^f(\mathbf{s}_k), \quad \text{for } i \in S_f \\ A_j^b(\mathbf{y}_{T-k}, \mathbf{s}_{T-k}, \mathbf{a}_{T-k}) &= \epsilon_j^b \; r_j^b(\mathbf{y}_{T-k}, \mathbf{a}_{T-k}) + \gamma V_j^b(\mathbf{y}_{T-k-1}, \mathbf{s}_{T-k-1}) - V_j^b(\mathbf{y}_{T-k}, \mathbf{s}_{T-k}), \quad \text{for } j \in S_b. \end{aligned} \tag{19}$$

We then apply the FB-MOAC algorithm with the updated advantage functions. Note that this re-scaling does not lead to a linear preference due to Remark 3.4. We thus use different preference parameters to steer the learning process toward different regions of the Pareto front. It is also important to highlight that the scalarization technique cannot be applied on the forward and backward rewards to formulate a single reward, since the resulting reward would depend on both the forward and backward states. As a result, a state-coupled FB-MDP would occur and Lemma 3.8 would no longer hold. This further motivates using multi-objective optimization to find the Pareto-optimal solutions.

The non-linear re-scaling mechanism described above allows to characterize the Pareto-front of a problem. Note that theorems 4.1 and B.4 guarantee convergence to (locally) Pareto-optimal solutions. On the other hand,

theorem B.1 ensures that the expected losses monotonically decrease for any preference policy. Consequently, the convergence to a (locally) Pareto-optimal solution is preserved regardless of the different preferences. These considerations explain that the mechanism in Equation (19) allows to derive locally Pareto-optimal solutions for the case of Lipschitz-smooth losses; under the additional assumption of strong convexity of the losses, the mechanism even obtains the actual Pareto-optimal solutions. An evaluation of the proposed mechanism is provided in Section E.

5 Evaluation

FB-MDPs find application in stochastic optimal control problems driven by forward-backward stochastic differential equations (FB-SDEs) and networked systems (Zabihi et al., 2023). Accordingly, we evaluate FB-MOAC against the state of the art through diverse representative problems in these domains: mathematical finance, as an example of how a FB-SDE-driven stochastic control problem can be solved by FB-MOAC; and cache-assisted content delivery in wireless networks. Section D provides an additional use case in the context of computation offloading through an edge (cloud) server. The code of FB-MOAC is available at: https://anonymous.4open.science/r/FBMOAC-2025.

5.1 Use Case: Mathematical Finance

We consider an investment-consumption problem (Ma & Yong, 1999; El Karoui, 1997) In particular, we consider a stochastic optimal control problem driven by a forward-backward stochastic differential equation (FB-SDE), which is then discretized according to the method in Section E.1 to find an optimal solution with the FB-MOAC algorithm.

5.1.1 System Model

A financial market consists of n risky assets whose prices follow the following F-SDEs:

$$dp_n(t) = p_n(t)\big(r_n^{\text{app}}(t)dt + \langle \boldsymbol{\sigma}_n^{\text{vol}}(t), d\boldsymbol{\beta}(t)\rangle\big), \quad p_n(0) > 0,$$

for $n \in \{1, \dots, N\}$, where $\boldsymbol{\beta}(t) \in \mathbb{R}^N$ is the Wiener process with identity diffusion matrix, $r_n^{\text{app}}(t)$ is the instantaneous appreciation rate, and $\boldsymbol{\sigma}_n^{\text{vol}}(t) \in \mathbb{R}^N$ is the asset volatility. A trader invests in risky assets by fractional investments $\{0 \leq \phi_n(t) \leq 1\}_{n=1}^N$ or borrow / lend money with an interest rate $r^{\text{int}}(t)$. Hence, the wealth $w(t)$ of the trader with consumption plan $c(t)$ can be obtained by a F-SDE:

$$dw(t) = \left(r^{\text{int}}(t)w(t) + \sum_{n=1}^{N} w(t)\phi_n(t)\left(r_n^{\text{app}}(t) - r_n^{\text{int}}(t) - c(t)\right)\right)dt + \sum_{n=1}^{N} w(t)\phi_n(t)\langle \boldsymbol{\sigma}_n^{\text{vol}}(t), d\boldsymbol{\beta}(t)\rangle, \tag{20}$$

with $w(0) = w_0$ where w_0 is the initial wealth. Note that $\{\phi_n(t)\}_{n=1}^N$ is called the investment portfolio, with $\sum_{n=0}^N \phi_n(t) = 1$.

Then, an utility process $u(t)$ of the investor is taken into account. This process at time t depends on the consumption plan $c(t)$ and the future utility, and is described by the following B-SDE:

$$du(t) = -f^{\text{gen}}(c(t), u(t), z(t))dt + \langle \mathbf{z}(t), d\boldsymbol{\beta}(t)\rangle, \;\; u(T) = f^{\text{fin}}(w(T)), \tag{21}$$

where $f^{\text{gen}}(\cdot)$ is the generator function, $\mathbf{z} \in \mathbb{R}^N$ is the control process of the backward dynamics, T is the finite horizon, and $f^{\text{fin}}(\cdot)$ is the final utility function. The objective of this problem is to optimize the initial backward state $u(0)$ by designing an optimal portfolio and consumption plan. This is formulated based on the following stochastic optimal control problem:

$$\begin{aligned} \max_{\{\phi_n(t)\}_{n=0}^N,\, c(t)} \quad & \mathbb{E}\big\{f^{\text{fin}}(w(T)) + \int_0^T f^{\text{gen}}(c(t), u(t), z(t))dt\big\}, \\ \text{s.t.} \quad & \text{FB-SDE (20) and (21).} \end{aligned} \tag{22}$$

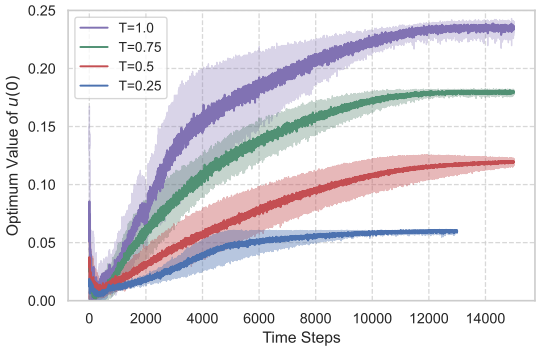

(a)

Risky assets N	**FB-MOAC**			**Approach in Ji et al. (2022b; 2020)**		
	T=0.50	T=0.75	T=1.00	T=0.50	T=0.75	T=1.00
10	0.121	0.182	0.241	0.122	0.182	0.242
20	0.122	0.181	0.240	0.122	0.178	0.242
50	0.120	0.180	0.235	0.121	0.181	0.237

(b)

Figure 2: Evaluation in a stochastic optimal control problem: (a) performance of FB-MOAC for $N = 50$ and for different horizons and (b) comparison of the optimal investor utility $u(0)$ against the state of the art.

So as to apply FB-MOAC, we discretize this stochastic optimal control problem with the Euler-Maruyama scheme (Kloeden & Platen, 1992) with a step-size $\Delta t = T/N^{\text{dis}}$. Therefore, the forward and backward states are the wealth $w(t)$ and utility process $u(t)$, respectively, and the backward reward is $\mathbb{E}\{f^{\text{fin}}(w(T)) + \sum_{i=0}^{N^{\text{dis}}} f^{\text{gen}}\big(c(i\Delta t), u(i\Delta t), z(i\Delta t)\big)\Delta t\}$.

5.1.2 Experiment Setup and Hyper-parameters

We use the same settings as those in (Ji et al., 2022a). The number of assets is $N \in \{10, 20, 50\}$, the generator function $f^{\text{gen}}(c(t), u(t), z(t)) = -0.05u(t) + c(t) - c(t)^2$, the final utility function $f^{\text{fin}}(x) = \exp(-x)$, the interest rate $r^{\text{int}}(t) = 0.03$, the appreciation rate $r^{\text{app}}(t) = 0.05$, the volatility $\boldsymbol{\sigma}_n^{\text{vol}} = 0.1\mathbf{I}_n$ for $n \in \{1, \ldots, N\}$, the finite horizon $T \in \{0.5, 0.75, 1.0\}$, and the initial wealth $x_0 = 100$.

As this problem only entails a backward reward, we only establish the backward-critic network; moreover, we set $N_{\text{MCS}} = 1$, the number of neurons in the hidden layer for the actor and critics to 8, the actor and bidirectional critic learning rates 2×10^{-2}, and the smoothing factor $\gamma_{\text{mov}} = 1$. We use the Dirichlet distribution for $\{\phi_n(t)\}_{n=0}^{N}$ to jointly motivate the exploration and satisfy $\sum_{n=0}^{N} \phi_n(t) = 1$. Finally, the rectified linear unit (ReLU) activation function is used for the neurons connection, the number of neurons in the hidden layer for the actor and critics is 100, the actor and forward / bidirectional critic learning rates are 3×10^{-4}, and the smoothing factor is $\gamma_{\text{mov}} = 0.95$.

5.1.3 Performance Evaluation

Figure 2a shows the performance of FB-MOAC as a function of time steps for different values of finite horizon $T \in \{0.5, 0.75, 1.0\}$. For comparison purposes, we consider the approaches in (Ji et al., 2022b; 2020), which develop deep learning methods by focusing on stochastic control theory and incorporate the system dynamics a priori for the optimization purposes. In contrast, FB-MOAC learns multivariate rewards for FB-MDPs *without* knowing the transition probability of the underlying dynamics. Table 2b compares FB-MOAC against state of the art in terms of the optimal initial investor utility $u(0)$. The FB-MOAC solution is close to the values obtained by (Ji et al., 2022b; 2020) for different values of T *despite* treating the system dynamics as a black-box during the learning process. This demonstrates the ability of the proposed algorithm to find an optimal solution for environments characterized as FB-MDPs, thereby broadening its application to a variety of stochastic optimal control problems described by FB-SDEs.

5.2 Case Study: Edge Caching

We now consider a real-world forward-backward multi-task problem in the context of edge caching (Nomikos et al., 2022). For conciseness, the rest of the section omits details that can be found in Section C.

5.2.1 System Model

The environment is a wireless network with cache-equipped serving-nodes (SNs) and fixed users requesting N contents items from them. The network operates over time slots indexed by $t \in \{1, \dots, T\}$, where T is the total time duration. A given user makes a single content request at every time slot, but its content preference changes in the subsequent time slot. Each SN multicasts popular contents to users at the start of each time slot, aiming to satisfy the requests of as many users as possible. The transmission at time-slot t is completed within a duration of $d(t)$ seconds. A transmission outage may occur with probability $\{O_n(\mathbf{a}(t), t)\}_{n=1}^N$, where $\mathbf{a}(t)$ denotes the *action* parameters of the network based on which it can control the outage. These include the radio resource allocation and the availability of cached content at SNs. Note that $\{O_n(\mathbf{a}(t), t)\}_{n=1}^N$ indicates the probability that the users cannot receive content n. As a result, some users fail to receive the requested content in the current time slot and their requests are deferred to the subsequent one. Hence, each time slot sees a distribution of users accounting for the repeated requests and a distribution describing the new preferences on contents. This leads to a time-varying model for the request probability of content n, $p_n^{\text{req}}(t)$. Requests for content can span multiple time-slots until successfully fulfilled, thereby affecting the expected latency to receive them. Such an expected latency $L_n(t)$ for the successful delivery of content n follows these dynamics (please refer to Section C for more details):

$$L_n(\mathbf{a}(t), t) = \Big(d(t) + L_n(\mathbf{a}(t+1), t+1)\Big) O_n(\mathbf{a}(t), t) + \frac{d(t)}{2}\big(1 - O_n(\mathbf{a}(t), t)\big), \quad L_n(\mathbf{a}(T), T) = 0, \tag{23}$$

where $d(t)$ is the duration of time-slot t in seconds, and we have $L_n(\mathbf{a}(T), T) = 0$ since system operations finish at $t = T$ and the users do not need to wait any longer. Equation (23) represents a **backward dynamics**, with the backward state vector $\mathbf{y}(t) = \mathbf{L}(\mathbf{a}(t), t)$ and the action vector $\mathbf{a}(t)$. Note that this model fully captures the trade-offs involved in the delay dynamics and differs from the conventional formalism that does not provide a continuum model when accounting for successive slots; for the delivery without outage, the expected latency simply becomes $L_n(t) = \frac{d(t)}{2}$, as its realizations follow a uniform distribution with values between 0 and $d(t)$.

Equation (23) may suggest that it is possible to convert it to a standard forward dynamics. For this purpose, we can consider a variable transformation $K_n(T-t) := L_n(\mathbf{a}(t), t)$ as well as a time transformation $t' := T - t$. We can then obtain the following forward dynamics on $K_n(t')$:

$$K_n(t') = \big(d(T-t') + K_n(t'-1)\big) O_n(\mathbf{a}(T-t'), T-t') + \frac{d(T-t')}{2}\big(1 - O_n(\mathbf{a}(T-t'), T-t')\big), \quad \text{for } t' \geq 1,$$

with $K_n'(0) = 0$. However, this shows a non-standard MDP, as the state $K_n(t')$ depends on the far future of action $\mathbf{a}_n(T-t')$ that cannot be revealed by moving forward in time. This argument aligns with Theorem 3.6.

Equation (23) also shows that for a full-error transmission scheme (i.e., with the outage equal to one) $L_n(t) = d(t) + L_n(t+1)$ holds, which means that the expected latency maximally accumulates as one goes backwards in time. This is expected, as no successful receptions take place. Moreover, it is worth stressing that minimizing the expected latency (23) enables to *optimally* keep track of the *precise* time slot at which requests are finally fulfilled. Alternatively, one could track the service time of requests to prioritize those that have waited longer. However, this oversimplifies the problem and fails to account for the complex interactions within the system, leading to a sub-optimal solution. Additional explanation is provided in Section 5.2.3.

The problem is therefore modeled as a FB-MDP, coupling forward and backward dynamics through system actions, where the action space is $[0, 1]^n \times [0, \infty]^n$ with n the number of contents.

Three widely-used *network performance metrics* (Li et al., 2018b) are considered as reward functions to design an optimal policy: the quality of service $r_{\text{QoS}}(\cdot)$; the total bandwidth consumption $r_{\text{BW}}(\cdot)$; and the overall expected latency $r_{\text{Lat}}(\cdot)$. The QoS determines the overall probability of unsatisfied UEs and is

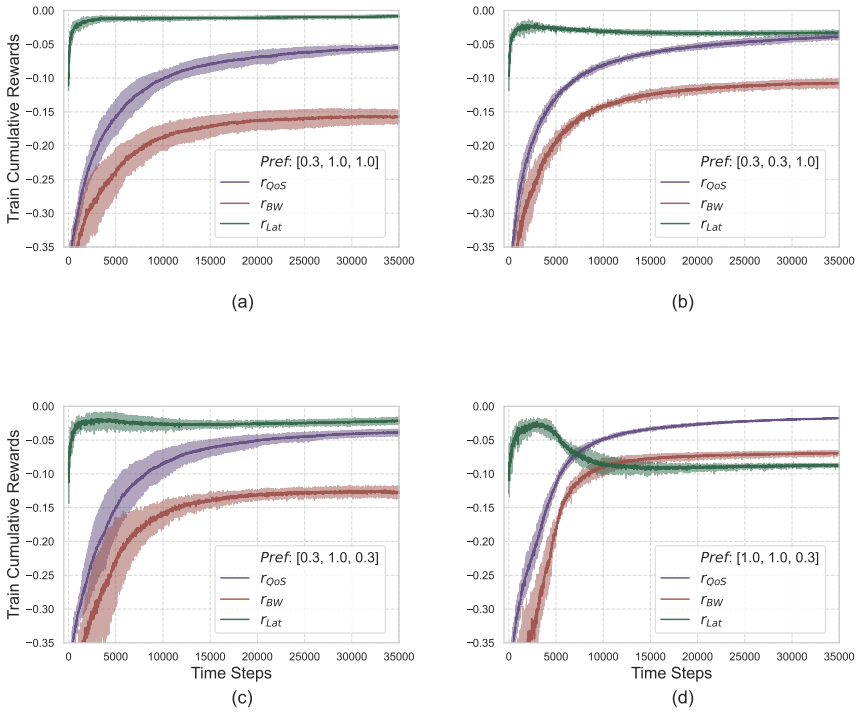

Figure 3: Pareto-optimal solutions in the edge caching use case for different settings of the preference parameters $\boldsymbol{\epsilon} = [\boldsymbol{\epsilon}^f, \epsilon^b]$: (a) $[0.3, 1.0, 1.0]$, (b) $[0.3, 0.3, 1.0]$, (c) $[0.3, 1.0, 0.3]$, and (d) $[1.0, 1.0, 0.3]$. Note that these solutions are Pareto-optimal as none of them dominates the others.

given by $r_{\text{QoS}}(t) = -\sum_{n=1}^{N} p_n^{\text{req}}(t) O_n\big(\mathbf{a}(t), t\big),\ 0 \leq -r_{\text{QoS}}(t) \leq 1$, namely, the likelihood of a UE request remaining unfulfilled during the multicast transmission at time-slot t. The total bandwidth consumption is $r_{\text{BW}}(t) = -W\big(\mathbf{a}(t), t\big) = -\sum_{n=1}^{N} w_n(t)$, where $W\big(\cdot\big)$ represents the total bandwidth consumption for the network. Finally, the overall expected latency is $r_{\text{Lat}}(t) = -\sum_{n=1}^{N} p_n^{\text{req}}(t) L_n(\mathbf{a}(t), t)$, with $L_n(t)$ obtained from Equation (23). Note that these rewards compete with each other. For instance, reducing r_{BW} requires increasing w_n which, in turn, decreases the outage O_n. Furthermore, a decrease in O_n makes r_{QoS} grow but reduces the latency L_n which, in turn, increases r_{lat}.

Clearly, $r_{\text{QoS}}(t)$ and $r_{\text{BW}}(t)$ relate to the forward state, and constitute the forward bivariate reward function $\boldsymbol{r}^f(t) = [r_{\text{QoS}}(t), r_{\text{BW}}(t)]$. Instead, $r_{\text{Lat}}(t)$ relates to the backward state, and constitutes a backward univariate reward function $r^b(t) = r_{\text{Lat}}(t)$.

5.2.2 Experiment Setup and Hyper-parameters

We select the following parameters for the considered environment. The number of content items is set to $N = 200$, the spatial intensity of the SNs to $\lambda_{\text{sn}} = 100$ points/km^2, and the transmission rate to 1 Mbps. The total number of time slots is $T = 256$. For the content popularity, we use time-varying Zipf distributions (Li et al., 2018a).

As for *FB-MOAC*, three separate sets of NNs representing the multi-objective actor in addition to the forward-critic and the backward-critic networks. We use $N_{\text{MCS}} = 4$ many NNs for the forward critic as well as for the backward critic. The forward critic outputs two values representing the reward-specific state-value functions $V^f_{\boldsymbol{\phi},j}(\cdot)$, related to $r_{\text{QoS}}(\cdot)$ and $r_{\text{BW}}(\cdot)$. On the other hand, the backward critic outputs one value representing the state-value functions $V^b_{\boldsymbol{\psi}}(\cdot)$, related to $r_{\text{Lat}}(\cdot)$. We set the actor and critic learning rates to 4×10^{-4} and the discount factor to $\gamma = 0.92$.

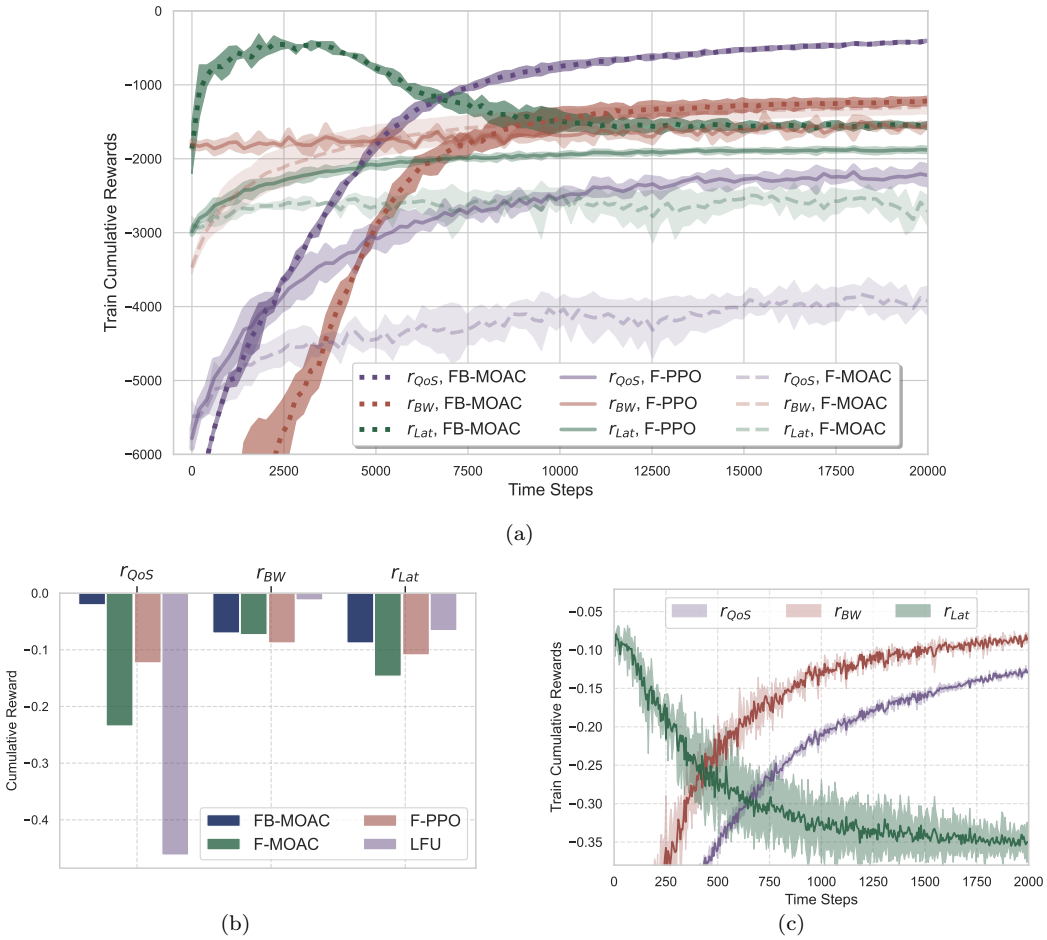

Figure 4: Performance of FB-MOAC for the edge caching use case: (a) performance comparison against forward learning with F-PPO, F-MOAC, and LFU; (b) comparison between the test solution of FB-MOAC with those of F-PPO, F-MOAC, and LFU; (c) learning in absence of backward optimization.

5.2.3 Performance Evaluation

Figure 3 illustrates the learning results of FB-MOAC in deriving most of the Pareto-optimal solutions, i.e., the resulting solution of each figure does not dominate the others. Recall that Section 4.3 describes a mechanism for obtaining a Pareto-front; Section E further characterizes such a front for the use case considered here. For clarity, the performance metrics are *normalized* based on the value of r_{QoS}, so that they can be clearly shown in a single plot and more importantly the value of r_{QoS} shows the *average* percentage of failed requests. As the results of forward and backward rewards eventually evolve into a stable solution, the actor and the forward / bidirectional critics are effectively learned.

We consider three baselines for comparison: a widely-used rule-based approach for caching, the Least Frequently Used (LFU) strategy (Ahmed et al., 2013); and two learning-based algorithms by replacing the backward reward with a related one (for fairness) so that the backward MDP can be safely removed. Specifically, we manage the time slot during which requests are served by optimizing $d(t)$. We further leverage the fact that maximizing r_{QoS} reduces r_{Lat} based on Equation (23). Hence, we consider r_{QoS} and r_{BW} as forward rewards, replace the backward reward with optimizing $d(t)$, then use the baseline algorithm PPO (Schulman et al., 2017a) as well as F-MOAC, derived from FB-MOAC by excluding the backward learning mechanism. Notably, F-MOAC is considered a multi-objective extension of the baseline algorithm A2C (Grondman et al., 2012). We term the resulting solutions of these strategies as F-PPO and F-MOAC, since they are developed for forward MDPs. Figure 4a compares the training performance of FB-MOAC

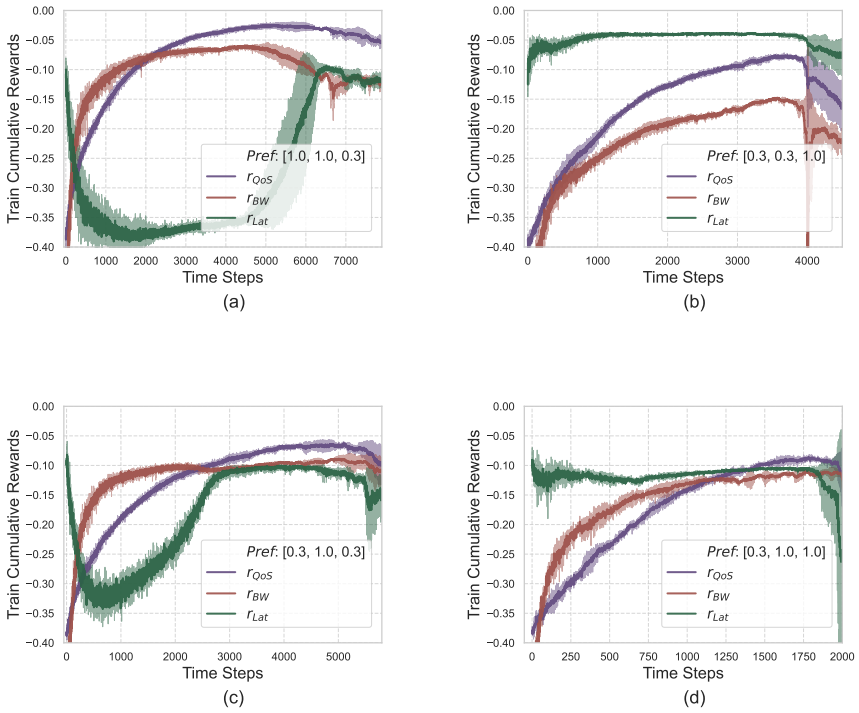

Figure 5: Train performance when single-objective optimization is used with different values of the scalarization settings $\mathbf{s} = [\mathbf{s}^f, s^b]$: (a) $[0.3, 0.3, 1.0]$, (b) $[1.0, 1.0, 0.3]$, (c) $[0.3, 1.0, 0.3]$ and (d) $[0.3, 1.0, 1.0]$.

against baselines F-PPO and F-MOAC, in terms of normalized rewards, while Figure 4b shows the solutions of these algorithms during test. We select a solution for FB-MOAC among different ones by prioritizing r_{QoS}. Instead, we learn forward rewards and additionally optimize $d(t)$ for the two baselines (F-PPO and F-MOAC) to achieve a r_{Lat} comparable (or slightly worse) to that of FB-MOAC. The results show that FB-MOAC remarkably outperforms both F-MOAC and F-PPO in terms of all rewards. This means that FB-MOAC strategy can fulfill the content requests considerably better than forward-only strategies. Specifically, more than 15% of the content items are lost due to the values of quality of service in both F-PPO and F-MOAC, whereas the failure rate of FB-MOAC is only **2%**. Moreover, FB-MOAC gives a comparable or better policy than those obtained by F-PPO and F-MOAC. Furthermore, the solution of FB-MOAC Pareto-dominates those of F-PPO and F-MOAC. The LFU policy does not benefit from any preference settings with respect to rewards. Although, it is better than FB-MOAC from the bandwidth-consumption r_{BW} perspective; it is very unreliable because 45% of the requests fail. These findings show the importance of explicitly incorporating the backward MDP instead of trying to remove it through adjustments to the backward rewards. They also demonstrate the effectiveness of the proposed FB-MOAC algorithm in solving the respective FB-MDP problem.

5.2.4 Ablation Study

We now conduct an ablation study to assess the benefit of the backward evaluation / optimization in FB-MOAC. For this purpose, we first disable the backward evaluation of the algorithm and only consider the forward actor and critic losses. Figure 4c shows the resulting rewards as a function of time steps, highlighting that r_{lat} does not improve over time. As a consequence, the results establish the necessity of the backward evaluation / optimization in FB-MOAC.

We further carry out another ablation study to evaluate the impact of the multi-objective procedure in Equations (15), (16) and (18) on the performance. For this purpose, we replace the proposed multi-objective optimization with a single-objective one accompanied with a linear scalarization technique. Specifically, we

update the actor parameter $\boldsymbol{\theta}$ using the following rule:

$$\boldsymbol{\theta} \leftarrow \boldsymbol{\theta} - \mu\big(\sum_{j \in S_f} s_j^f \nabla_{\boldsymbol{\theta}} \hat{J}_j^f(\boldsymbol{\theta}, \boldsymbol{\phi}) + \sum_{j \in S_b} s_j^b \nabla_{\boldsymbol{\theta}} \hat{J}_j^b(\boldsymbol{\theta}, \boldsymbol{\psi}) \big),$$

where $\mathbf{s}^f = [\{s_j^f\}_{j \in S_f}] \in [0.1, 1]^{|S_f|}$ and $\mathbf{s}^f = [\{s_j^b\}_{j \in S_b}] \in [0.1, 1]^{|S_b|}$ are the scalarization settings. Accordingly, Figure 5 shows the train performance of this approach for different scalarization settings $[\mathbf{s}^f, s^b]$: $[0.3, 0.3, 1.0]$, $[1.0, 1.0, 0.3]$ and $[0.3, 1.0, 0.3]$. Clearly, the single-objective mechanism fails to provide stable solutions, in contrast with the proposed multi-objective approach (see also Figure 3).

6 Conclusion and Limitations

We introduced the notion of forward-backward Markov decision processes (FB-MDPs), a class of MDPs that cannot be expressed as standard MDPs. We then obtained an optimality condition for the solution of FB-MDPs based on which we devised a multi-objective RL algorithm called FB-MOAC. We analytically characterized the optimality and convergence of FB-MOAC, then conducted an extensive evaluation in two diverse use cases to demonstrate its effectiveness.

As a limitation, our mechanism targeted FB-MDP problems wherein forward and backward dynamics are purely coupled within the action space. Addressing fully-coupled FB-MDPs is an interesting direction for future work.

References

Abbas Abdolmaleki, Jost Tobias Springenberg, Yuval Tassa, Remi Munos, Nicolas Heess, and Martin Riedmiller. Maximum a posteriori policy optimisation. In *International Conference on Learning Representations*, 2018.

Abbas Abdolmaleki, Sandy H. Huang, Leonard Hasenclever, Michael Neunert, H. Francis Song, Martina Zambelli, Murilo F. Martins, Nicolas Heess, Raia Hadsell, and Martin Riedmiller. A distributional view on multi-objective policy optimization. In *International Conference on Machine Learning*, 2020.

Mohamed Ahmed, Stefano Traverso, Paolo Giaccone, Emilio Leonardi, and Saverio Niccolini. Analyzing the performance of LRU caches under non-stationary traffic patterns. eprint arXiv 1301.4909, 2013.

Mohsen Amidzadeh, Hanan Al-Tous, Olav Tirkkonen, and Junshan Zhang. Joint cache placement and delivery design using reinforcement learning for cellular networks. In *Vehicular Technology Conference*, pp. 1–6, 2021.

Mohsen Amidzadeh, Hanan Al-Tous, Giuseppe Caire, and Olav Tirkkonen. Caching in cellular networks based on multipoint multicast transmissions. *IEEE Transactions on Wireless Communications*, 22(4): 2393–2408, 2023.

Feng Archibald, RichardBao and Jiongmin Yong. A stochastic gradient descent approach for stochastic optimal control. *East Asian Journal on Applied Mathematics*, 10(4):635–658, 2020. ISSN 2079-7370.

Richard Archibald, Feng Bao, and Jiongmin Yong. A stochastic maximum principle approach for reinforcement learning with parameterized environment. *Journal on Computational Physics*, 488:112238, 2023.

Shuangwu Chen, Zhen Yao, Xiaofeng Jiang, Jian Yang, and Lajos Hanzo. Multi-agent deep reinforcement learning-based cooperative edge caching for ultra-dense next-generation networks. *IEEE Transactions on Communications*, 69(4):2441–2456, 2021. doi: 10.1109/TCOMM.2020.3044298.

Xi Chen, Ali Ghadirzadeh, Mårten Björkman, and Patric Jensfelt. Meta-learning for multi-objective reinforcement learning. In *IEEE/RSJ International Conference on Intelligent Robots and Systems*, pp. 977–983, 2019a.

Xianfu Chen, Honggang Zhang, Celimuge Wu, Shiwen Mao, Yusheng Ji, and Mehdi Bennis. Optimized computation offloading performance in virtual edge computing systems via deep reinforcement learning. *IEEE Internet of Things Journal*, 6(3):4005–4018, 2019b.

Zhixiong Chen, Wenqiang Yi, Atm S. Alam, and Arumugam Nallanathan. Dynamic task software caching-assisted computation offloading for multi-access edge computing. *IEEE Transactions on Communications*, 70(10):6950–6965, 2022. doi: 10.1109/TCOMM.2022.3200109.

Ashley D Edwards, Laura Downs, and James C Davidson. Forward-backward reinforcement learning. *arXiv preprint arXiv:1803.10227*, 2018.

N. El Karoui. Backward stochastic differential equations in finance. *Mathematical Finance*, 7(1):1–31, 1997.

Zuyue Fu, Zhuoran Yang, and Zhaoran Wang. Single-timescale actor-critic provably finds globally optimal policy. In *International Conference on Learning Representations, ICLR*, 2021.

Anirudh Goyal, Philemon Brakel, William Fedus, Soumye Singhal, Timothy P. Lillicrap, Sergey Levine, Hugo Larochelle, and Yoshua Bengio. Recall traces: Backtracking models for efficient reinforcement learning. In *International Conference on Learning Representations, ICLR*. OpenReview.net, 2019.

Ivo Grondman, Lucian Busoniu, Gabriel A. D. Lopes, and Robert Babuska. A survey of actor-critic reinforcement learning: Standard and natural policy gradients. *IEEE Trans. on Systems, Man, and Cybernetics*, 42(6):1291–1307, 2012.

S. Hamadene and J. P. Lepeltier. Zero-sum stochastic differential games and backward equations. *Syst. Control Lett.*, 24(4):259–263, March 1995. ISSN 0167-6911. doi: 10.1016/0167-6911(94)00011-J.

Max Jaderberg, Wojciech M Czarnecki, Iain Dunning, Luke Marris, Guy Lever, Antonio Garcia Castaneda, Charles Beattie, Neil C Rabinowitz, Ari S Morcos, Avraham Ruderman, et al. Human-level performance in first-person multiplayer games with population-based deep reinforcement learning. *arXiv preprint arXiv:1807.01281*, 2018.

S. Ji, S. Peng, Y. Peng, and X. Zhang. Three algorithms for solving high-dimensional fully coupled fbsdes through deep learning. *IEEE Intelligent Systems*, 35(03):71–84, may 2020.

Shaolin Ji, Shige Peng, Ying Peng, and Xichuan Zhang. A deep learning method for solving stochastic optimal control problems driven by fully-coupled fbsdes. *arXiv:2204.05796 [math.OC]*, 2022a. URL `https://arxiv.org/abs/2204.05796`.

Shaolin Ji, Shige Peng, Ying Peng, and Xichuan Zhang. Solving stochastic optimal control problem via stochastic maximum principle with deep learning method. *Journal of Scientific Computing*, 93(1):30, 2022b. doi: 10.1007/s10915-022-01979-5.

Wei Jiang, Daquan Feng, Yao Sun, Gang Feng, Zhenzhong Wang, and Xiang-Gen Xia. Proactive content caching based on actor–critic reinforcement learning for mobile edge networks. *IEEE Transactions on Cognitive Communications and Networking*, 8(2):1239–1252, 2022. doi: 10.1109/TCCN.2021.3130995.

Sham M. Kakade. A natural policy gradient. In *Advances in Neural Information Processing Systems*, 2002.

Sajad Khodadadian, Prakirt Raj Jhunjhunwala, Sushil Mahavir Varma, and Siva Theja Maguluri. On linear and super-linear convergence of natural policy gradient algorithm. *Systems & Control Letters*, 164:105214, 2022.

Gokhan Kirlik and Serpil Sayın. A new algorithm for generating all nondominated solutions of multiobjective discrete optimization problems. *European Journal of Operational Research*, 232(3):479–488, 2014.

Peter E Kloeden and Eckhard Platen. *Numerical Solution of Stochastic Differential Equations*. Springer, 1992.

Hang Lai, Jian Shen, Weinan Zhang, and Yong Yu. Bidirectional model-based policy optimization. In *International Conference on Machine Learning, ICML*, volume 119 of *Proceedings of Machine Learning Research*, pp. 5618–5627. PMLR, 2020.

K. Li, C. Yang, Z. Chen, and M. Tao. Optimization and analysis of probabilistic caching in n-tier heterogeneous networks. *IEEE Trans. Wireless Commun.*, 17(2):1283–1297, 2018a.

Liying Li, Guodong Zhao, and Rick S. Blum. A survey of caching techniques in cellular networks: Research issues and challenges in content placement and delivery strategies. *IEEE Communications Surveys and Tutorials*, 20(3):1710–1732, 2018b.

Timothy P. Lillicrap, Jonathan J. Hunt, Alexander Pritzel, Nicolas Heess, Tom Erez, Yuval Tassa, David Silver, and Daan Wierstra. Continuous control with deep reinforcement learning. In *International Conference on Learning Representations, ICLR*, 2016.

Yi Liu, Huimin Yu, Shengli Xie, and Yan Zhang. Deep reinforcement learning for offloading and resource allocation in vehicle edge computing and networks. *IEEE Transactions on Vehicular Technology*, 68(11): 11158–11168, 2019.

Jin Ma and Jiongmin Yong. *Forward-Backward Stochastic Differential Equations and their Applications*, volume 1702 of *Lecture Notes in Mathematics*. Springer, 1999.

Pingchuan Ma, Tao Du, and Wojciech Matusik. Efficient continuous pareto exploration in multi-task learning. In *International Conference on Machine Learning*, ICML, 2020.

Volodymyr Mnih, Koray Kavukcuoglu, David Silver, Alex Graves, Ioannis Antonoglou, Daan Wierstra, and Martin Riedmiller. Playing atari with deep reinforcement learning. *arXiv preprint arXiv:1312.5602*, 2013.

Volodymyr Mnih, Koray Kavukcuoglu, David Silver, Andrei A Rusu, Joel Veness, Marc G Bellemare, Alex Graves, Martin Riedmiller, Andreas K Fidjeland, Georg Ostrovski, et al. Human-level control through deep reinforcement learning. *Nature*, 518(7540):529–533, 2015.

Hossam Mossalam, Yannis M. Assael, Diederik M. Roijers, and Shimon Whiteson. Multi-objective deep reinforcement learning. preprint ArXiv 1610.02707, 2016.

Nikolaos Nomikos, Spyros Zoupanos, Themistoklis Charalambous, and Ioannis Krikidis. A survey on reinforcement learning-aided caching in heterogeneous mobile edge networks. *IEEE Access*, 10:4380–4413, 2022. doi: 10.1109/ACCESS.2022.3140719.

Jan Peters and Stefan Schaal. Natural actor-critic. *Neurocomputing: An International Journal*, 71(7-9): 1180–1190, 2008.

Shuang Qiu, Zhuoran Yang, Jieping Ye, and Zhaoran Wang. On finite-time convergence of actor-critic algorithm. *IEEE Journal on Selected Areas in Information Theory*, 2(2):652–664, 2021.

Lillian M Rigoli, Gaurav Patil, Hamish F Stening, Rachel W Kallen, and Michael J Richardson. Navigational behavior of humans and deep reinforcement learning agents. *Frontiers in Psychology*, 12:725932, 2021.

John Schulman, Filip Wolski, Prafulla Dhariwal, Alec Radford, and Oleg Klimov. Proximal policy optimization algorithms. *CoRR*, abs/1707.06347, 2017a. URL `http://arxiv.org/abs/1707.06347`.

John Schulman, Filip Wolski, Prafulla Dhariwal, Alec Radford, and Oleg Klimov. Proximal policy optimization algorithms, 2017b.

Stefan Schäffler, Simon R. Schultz, and Klaus Weinzierl. Stochastic method for the solution of unconstrained vector optimization problems. *Journal of Optimization Theory and Applications*, 2002.

Richard S. Sutton and Andrew G. Barto. *Reinforcement Learning: An Introduction*. The MIT Press, 2018.

Gabriel Turinici. The convergence of the stochastic gradient descent (SGD): a self-contained proof. Technical report, 2021.

Jianhao Wang, Wenzhe Li, Haozhe Jiang, Guangxiang Zhu, Siyuan Li, and Chongjie Zhang. Offline reinforcement learning with reverse model-based imagination. In *Annual Conference on Neural Information Processing Systems, NeurIPS*, pp. 29420–29432, 2021.

Yifei Wei, F. Richard Yu, Mei Song, and Zhu Han. Joint optimization of caching, computing, and radio resources for fog-enabled iot using natural actor–critic deep reinforcement learning. *IEEE Internet of Things Journal*, 6(2):2061–2073, 2019. doi: 10.1109/JIOT.2018.2878435.

Tengyu Xu, Zhe Wang, and Yingbin Liang. Improving sample complexity bounds for (natural) actor-critic algorithms. *Advances in Neural Information Processing Systems*, 33:4358–4369, 2020.

Ling Yang, Zhilong Zhang, Yang Song, Shenda Hong, Runsheng Xu, Yue Zhao, Wentao Zhang, Bin Cui, and Ming-Hsuan Yang. Diffusion models: A comprehensive survey of methods and applications. *ACM Comput. Surv.*, 56(4), November 2023. ISSN 0360-0300. doi: 10.1145/3626235.

Runzhe Yang, Xingyuan Sun, and Karthik Narasimhan. A generalized algorithm for multi-objective reinforcement learning and policy adaptation. In *International Conference on Neural Information Processing Systems*, 2019.

Zhuoran Yang, Kaiqing Zhang, Mingyi Hong, and Tamer Başar. A finite sample analysis of the actor-critic algorithm. In *IEEE conference on decision and control, CDC*, pp. 2759–2764, 2018.

Jiongmin Yong. Forward-backward stochastic differential equations: Initiation, development and beyond. *Numerical Algebra, Control and Optimization*, 13(3):367–391, 2023. ISSN 2155-3289.

Zeinab Zabihi, Amir Masoud Eftekhari Moghadam, and Mohammad Hossein Rezvani. Reinforcement learning methods for computation offloading: A systematic review. *ACM Comput. Surv.*, 56(1), aug 2023. ISSN 0360-0300. doi: 10.1145/3603703. URL `https://doi.org/10.1145/3603703`.

Maryam Zare, Parham M Kebria, Abbas Khosravi, and Saeid Nahavandi. A survey of imitation learning: Algorithms, recent developments, and challenges. *arXiv preprint arXiv:2309.02473*, 2023.

Huixin Zhan and Yongcan Cao. Relationship explainable multi-objective optimization via vector value function based reinforcement learning. preprint ArXiv 1910.01919, 2019.

Fan Zhang, Guangjie Han, Li Liu, Miguel Martínez-García, and Yan Peng. Joint optimization of cooperative edge caching and radio resource allocation in 5G-enabled massive IoT networks. *IEEE Internet of Things Journal*, 8(18):14156–14170, 2021. doi: 10.1109/JIOT.2021.3068427.

Jianfeng Zhang. *Backward Stochastic Differential Equations: From Linear to Fully Nonlinear Theory*, volume 86 of *Probability Theory and Stochastic Modelling*. Springer, 2017.

Liangquan Zhang. A BSDE approach to stochastic differential games involving impulse controls and HJBI equation. *Journal of Systems Science and Complexity*, 35(3):766–801, 2022.

Huan Zhou, Zhenyu Zhang, Yuan Wu, Mianxiong Dong, and Victor C. M. Leung. Energy efficient joint computation offloading and service caching for mobile edge computing: A deep reinforcement learning approach. *IEEE Transactions on Green Communications and Networking*, 7(2):950–961, 2023. doi: 10.1109/TGCN.2022.3186403.

Shiji Zhou, Wenpeng Zhang, Jiyan Jiang, Wenliang Zhong, Jinjie GU, and Wenwu Zhu. On the convergence of stochastic multi-objective gradient manipulation and beyond. In Alice H. Oh, Alekh Agarwal, Danielle Belgrave, and Kyunghyun Cho (eds.), *Advances in Neural Information Processing Systems*, 2022.

SUPPLEMENTARY MATERIAL

A Proof of Lemma 3.8

Proof. We simply denote the conditional expectation $\mathbb{E}\{\cdot|\boldsymbol{\theta}\}$ by $\mathbb{E}\{\cdot\}$ for convenience. Accordingly, we have:

$$\nabla_{\boldsymbol{\theta}}\mathbf{J}^b(\boldsymbol{\theta}) = \nabla_{\boldsymbol{\theta}}\,\mathbb{E}_{\mathrm{P}_{\boldsymbol{\theta}}(\boldsymbol{\tau})}\left\{\sum_{k=0}^{T-1}\gamma^k \boldsymbol{r}^b(\mathbf{y}_{T-k},\mathbf{a}_{T-k})\right\} \tag{24}$$

$$\begin{aligned}
&\overset{a}{=}\ \mathbb{E}_{\mathrm{P}_{\boldsymbol{\theta}}(\boldsymbol{\tau})}\left\{\sum_{k=0}^{T-1}\gamma^k \boldsymbol{r}^b(\mathbf{y}_{T-k},\mathbf{a}_{T-k})\sum_{k=0}^{T-1}\nabla_{\boldsymbol{\theta}}\log\pi_{\boldsymbol{\theta}}(\mathbf{a}_{T-k}|\mathbf{s}_{T-k})\right\}\\
&\overset{b}{=}\mathbb{E}_{\mathrm{P}_{\boldsymbol{\theta}}(\boldsymbol{\tau})}\left\{\sum_{k=0}^{T-1}\nabla_{\boldsymbol{\theta}}\log\pi_{\boldsymbol{\theta}}(\mathbf{a}_{T-k}|\mathbf{s}_{T-k})\sum_{k'=k}^{T-1}\gamma^{k'-k}\boldsymbol{r}^b(\mathbf{y}_{T-k'},\mathbf{a}_{T-k'})\right\}\\
&\overset{c}{=}\sum_{k=0}^{T-1}\mathop{\mathbb{E}}_{\substack{\mathbf{y}_{T-k}\\ \mathbf{a}_{T-k}\\ \mathbf{s}_{T-k}}}\left\{\nabla_{\boldsymbol{\theta}}\log\pi_{\boldsymbol{\theta}}(\mathbf{a}_{T-k}|\mathbf{s}_{T-k})\underbrace{\mathbb{E}\left\{\sum_{k'=k}^{T-1}\gamma^{k'-k}\boldsymbol{r}^b(\mathbf{y}_{T-k'},\mathbf{a}_{T-k'})\Big|\mathbf{y}_{T-k},\mathbf{s}_{T-k},\mathbf{a}_{T-k}\right\}}_{Q^b(\mathbf{y}_{T-k},\mathbf{s}_{T-k},\mathbf{a}_{T-k})}\right\}\\
&\overset{d}{=}\sum_{k=0}^{T-1}\mathop{\mathbb{E}}_{\substack{\mathbf{y}_{T-k}\\ \mathbf{a}_{T-k}\\ \mathbf{s}_{T-k}}}\left\{\nabla_{\boldsymbol{\theta}}\log\pi_{\boldsymbol{\theta}}(\mathbf{a}_{T-k}|\mathbf{s}_{T-k})\Big(Q^b(\mathbf{y}_{T-k},\mathbf{s}_{T-k},\mathbf{a}_{T-k})-V^b(\mathbf{y}_{T-k},\mathbf{s}_{T-k})\Big)\right\}\\
&\overset{e}{=}\sum_{k=0}^{T-1}\mathop{\mathbb{E}}_{\substack{\mathbf{y}_{T-k}\\ \mathbf{a}_{T-k}\\ \mathbf{s}_{T-k}}}\left\{\nabla_{\boldsymbol{\theta}}\log\pi_{\boldsymbol{\theta}}(\mathbf{a}_{T-k}|\mathbf{s}_{T-k})\Big(\mathop{\mathbb{E}}_{\substack{\mathbf{y}_{T-k-1}\sim P_b(\cdot|\mathbf{y}_{T-k},\mathbf{a}_{T-k})\\ \mathbf{s}_{T-k-1}\sim P(\cdot|\mathbf{s}_{T-k})}}\{\boldsymbol{r}^b(\mathbf{y}_{T-k},\mathbf{a}_{T-k})+\gamma V^b(\mathbf{y}_{T-k-1},\mathbf{s}_{T-k-1})\}-V^b(\mathbf{y}_{T-k},\mathbf{s}_{T-k})\Big)\right\}\\
&=\sum_{k=0}^{T-1}\mathbb{E}\left\{\nabla_{\boldsymbol{\theta}}\log\pi_{\boldsymbol{\theta}}(\mathbf{a}_{T-k}|\mathbf{s}_{T-k})\big(\mathbf{r}^b(\mathbf{y}_{T-k},\mathbf{a}_{T-k})+\gamma V^b(\mathbf{y}_{T-k-1},\mathbf{s}_{T-k-1})-V^b(\mathbf{y}_{T-k},\mathbf{s}_{T-k})\big)\right\}\\
&=\mathbb{E}_{\mathrm{P}_{\boldsymbol{\theta}}(\boldsymbol{\tau})}\left\{\sum_{k=0}^{T-1}\nabla_{\boldsymbol{\theta}}\log\pi_{\boldsymbol{\theta}}(\mathbf{a}_{T-k}|\mathbf{s}_{T-k})\mathbf{A}^b(\mathbf{y}_{T-k},\mathbf{s}_{T-k},\mathbf{a}_{T-k})\right\},
\end{aligned} \tag{25}$$

where $V^b(\cdot,\cdot):\mathcal{Y}\times\mathcal{S}\to\mathbb{R}^{|S_b|}$, $Q^b(\cdot,\cdot,\cdot):\mathcal{Y}\times\mathcal{S}\times\mathcal{A}\to\mathbb{R}^{|S_b|}$ and $A^b(\cdot,\cdot,\cdot):\mathcal{Y}\times\mathcal{S}\times\mathcal{A}\to\mathbb{R}^{|S_b|}$ are the bidirectional state-value, backward action-value, and bidirectional advantage multivariate functions, respectively. We also have:

$$V^b(\mathbf{y}_{T-k},\mathbf{s}_{T-k}) := \mathbb{E}\left\{\sum_{k'=k}^{T-1}\gamma^{k'-k}\boldsymbol{r}^b(\mathbf{y}_{T-k'},\mathbf{a}_{T-k'})\Big|\mathbf{y}_{T-k},\mathbf{s}_{T-k}\right\}. \tag{26}$$

For (a), we used $\nabla_{\boldsymbol{\theta}}\mathrm{P}_{\boldsymbol{\theta}}(\boldsymbol{\tau}) = \mathrm{P}_{\boldsymbol{\theta}}(\boldsymbol{\tau})\ \nabla_{\boldsymbol{\theta}}\log\mathrm{P}_{\boldsymbol{\theta}}(\boldsymbol{\tau})$, and $\nabla_{\boldsymbol{\theta}}\log\mathrm{P}_{\boldsymbol{\theta}}(\boldsymbol{\tau}) = \sum_{k=0}^{T-1}\nabla_{\boldsymbol{\theta}}\log\pi_{\boldsymbol{\theta}}(\mathbf{a}_{T-k}|\mathbf{s}_{T-k})$ based on Equation (3). For (b), we considered the anti-causality; the current action does not affect the future of backward rewards, for (c), the definition of backward action-value functions is applied, for (d), including a bias term, here $V^b(\mathbf{y}_{T-k},\mathbf{s}_{T-k})$, does not change the result due to $\mathbb{E}_{\mathbf{a}_{T-k}\sim\pi_{\boldsymbol{\theta}}(\cdot|\mathbf{s}_{T-k})}\{\nabla_{\boldsymbol{\theta}}\log\pi_{\boldsymbol{\theta}}(\mathbf{a}_{T-k}|\mathbf{s}_{T-k})\}=\mathbf{0}$

and for (e) we derive the Bellman's equation for the backward action-value function as follows:

$$
\begin{aligned}
&Q^b(\mathbf{y}_{T-k}, \mathbf{s}_{T-k}, \mathbf{a}_{T-k}) \\
&= \int \mathbb{E}\left\{ \sum_{k'=k}^{T-1} \gamma^{k'-k} \boldsymbol{r}^b(\mathbf{y}_{T-k'}, \mathbf{a}_{T-k'}) \Big| \mathbf{y}_{T-k}, \mathbf{a}_{T-k}, \mathbf{y}_{T-k-1}, \mathbf{s}_{T-k}, \mathbf{s}_{T-k-1} \right\} P_b(\mathbf{y}_{T-k-1}|\mathbf{y}_{T-k}, \mathbf{a}_{T-k}) \times \\
&\qquad\qquad P(\mathbf{s}_{T-k-1}|\mathbf{s}_{T-k}) d\mathbf{y}_{T-k-1} d\mathbf{s}_{T-k-1} \\
&\overset{\alpha}{=} \int \left(\boldsymbol{r}^b(\mathbf{y}_{T-k}, \mathbf{a}_{T-k}) + \gamma \mathbb{E}\left\{ \sum_{k'=k+1}^{T-1} \gamma^{k'-k} \boldsymbol{r}^b(\mathbf{y}_{T-k'}, \mathbf{a}_{T-k'}) \Big| \mathbf{y}_{T-k-1}, \mathbf{s}_{T-k-1} \right\} \right) P_b(\mathbf{y}_{T-k-1}|\mathbf{y}_{T-k}, \mathbf{a}_{T-k}) \times \\
&\qquad\qquad P(\mathbf{s}_{T-k-1}|\mathbf{s}_{T-k}) d\mathbf{y}_{T-k-1} d\mathbf{s}_{T-k-1} \\
&= \mathop{\mathbb{E}}_{\substack{\mathbf{y}_{T-k-1} \sim P_b(\cdot|\mathbf{y}_{T-k}, \mathbf{a}_{T-k}) \\ \mathbf{s}_{T-k-1} \sim P(\cdot|\mathbf{s}_{T-k})}} \left\{ \boldsymbol{r}^b(\mathbf{y}_{T-k}, \mathbf{a}_{T-k}) + \gamma V^b(\mathbf{y}_{T-k-1}) \right\}, \qquad (27)
\end{aligned}
$$

where for (α) we considered that $(\mathbf{y}_{T-k-1}, \mathbf{s}_{T-k-1})$ is the only relevant information to compute the expectation $\mathbb{E}\left\{\sum_{k'=k+1}^{T-1} \gamma^{k'-k} \boldsymbol{r}^b(\mathbf{y}_{T-k'}, \mathbf{a}_{T-k'})\right\}$. The same strategy can be applied to obtain the Bellman's equation for the bidirectional state-value function as follows:

$$
V^b(\mathbf{y}_{T-k}, \mathbf{s}_{T-k}) = \mathop{\mathbb{E}}_{\substack{\mathbf{a}_{T-k} \sim \pi_{\boldsymbol{\theta}}(\cdot|\mathbf{s}_{T-k}) \\ \mathbf{y}_{T-k-1} \sim P_b(\cdot|\mathbf{y}_{T-k}, \mathbf{a}_{T-k}) \\ \mathbf{s}_{T-k-1} \sim P(\cdot|\mathbf{s}_{T-k})}} \left\{ \boldsymbol{r}^b(\mathbf{y}_{T-k}, \mathbf{a}_{T-k}) + \gamma V^b(\mathbf{y}_{T-k-1}, \mathbf{s}_{T-k-1}) \mid \boldsymbol{\theta} \right\}.
$$

Note that no distinct forward and backward Bellman optimality equations do exist for the FB-MDPs. However, a Bellman Pareto-optimality equation can be instead found. For this, we consider this fact that the forward and backward value functions become stationary when forward and backward transition probabilities are stationary. By recalling the notion of Pareto-optimality and Pareto front, we then define the Pareto-optimal forward and backward value functions as follows:

$$
\left[Q^{f^*}(\mathbf{s}, \mathbf{a}), Q^{b^*}(\mathbf{y}, \mathbf{s}, \mathbf{a})\right] \in \max_{\pi(\cdot|\cdot)} \left[Q^f(\mathbf{s}, \mathbf{a}), Q^b(\mathbf{y}, \mathbf{s}, \mathbf{a})\right], \qquad \left[V^{f^*}(\mathbf{s}), V^{b^*}(\mathbf{y})\right] \in \max_{\pi(\cdot|\cdot)} \left[V^f(\mathbf{s}), V^b(\mathbf{y}, \mathbf{s})\right],
$$

for all $(\mathbf{s}, \mathbf{y}, \mathbf{a}) \in \mathcal{S} \times \mathcal{Y} \times \mathcal{A}$, where $\left[Q^{f^*}(\mathbf{s}, \mathbf{a}), Q^{b^*}(\mathbf{y}, \mathbf{s}, \mathbf{a})\right]$ and $\left[V^{f^*}(\mathbf{s}), V^{b^*}(\mathbf{y}, \mathbf{s})\right]$ are the Pareto-optimal vector for the above multi-objective optimization. Now, we consider the following policy:

$$
\pi^*(\mathbf{a}|\mathbf{s}) = \begin{cases} 1, & \mathbf{a} \in \operatorname{argmax}_{\mathbf{a}} \left[Q^{f^*}(\mathbf{s}, \mathbf{a}), Q^{b^*}(\mathbf{y}, \mathbf{s}, \mathbf{a})\right] \\ 0, & \text{otherwise} \end{cases}.
$$

Note that here $\operatorname{argmax}_{\mathbf{a}} \left[Q^{f^*}(\mathbf{s}, \mathbf{a}), Q^{b^*}(\mathbf{y}, \mathbf{s}, \mathbf{a})\right]$ returns a set of vectors. We then have:

$$
\left[V^{f^*}(\mathbf{s}), V^{b^*}(\mathbf{y}, \mathbf{s})\right] \in \max_{\mathbf{a}} \left[Q^{f^*}(\mathbf{s}, \mathbf{a}), Q^{b^*}(\mathbf{y}, \mathbf{s}, \mathbf{a})\right].
$$

On the other hand, based on Equation (27) and the Bellman's equation for the forward action-value function, we can get:

$$
\begin{aligned}
Q^{f^*}(\mathbf{s}, \mathbf{a}) &= \mathop{\mathbb{E}}_{\mathbf{s}^+ \sim P_f(\cdot|\mathbf{s}, \mathbf{a})} \left\{ \boldsymbol{r}^f(\mathbf{s}, \mathbf{a}) + \gamma V^{f^*}\left(\mathbf{s}^+\right) \right\} \\
Q^{b^*}(\mathbf{y}, \mathbf{s}, \mathbf{a}) &= \mathop{\mathbb{E}}_{\substack{\mathbf{y}^- \sim P_b(\cdot|\mathbf{y}, \mathbf{a}) \\ \mathbf{s}^- \sim P(\cdot|\mathbf{s})}} \left\{ \boldsymbol{r}^b(\mathbf{y}, \mathbf{a}) + \gamma V^{b^*}\left(\mathbf{y}^-, \mathbf{s}^-\right) \right\},
\end{aligned}
$$

where $\mathbf{y}^-$ is the backward state preceding $\mathbf{y}$ and $\mathbf{s}^+$ is the forward state following $\mathbf{s}$. We therefore obtain the following Bellman Pareto-optimality equation:

$$
\left[V^{f^*}(\mathbf{s}), V^{b^*}(\mathbf{y}, \mathbf{s})\right] \in \max_{\mathbf{a}} \left[\mathop{\mathbb{E}}_{\mathbf{s}^+ \sim P_f(\cdot|\mathbf{s}, \mathbf{a})} \left\{ \boldsymbol{r}^f(\mathbf{s}, \mathbf{a}) + \gamma V^{f^*}\left(\mathbf{s}^+\right) \right\}, \mathop{\mathbb{E}}_{\substack{\mathbf{y}^- \sim P_b(\cdot|\mathbf{y}, \mathbf{a}) \\ \mathbf{s}^- \sim P(\cdot|\mathbf{s})}} \left\{ \boldsymbol{r}^b(\mathbf{y}, \mathbf{a}) + \gamma V^{b^*}\left(\mathbf{y}^-, \mathbf{s}^-\right) \right\} \right],
$$

This equation, termed as *Bellman Pareto-optimality equation*, provides a base to formulate dynamic programming algorithms for multi-objective FB-MOAC problems as well as motivates the usage of a multi-objective optimization framework.

□

B Convergence of the FB-MOAC Algorithm

In this section, we perform a comprehensive study of the convergence properties of the FB-MOAC algorithm. Our investigation starts by establishing of some foundational assumptions and the introduction of preliminary theorems and corollaries. Subsequently, we study the convergence analysis for two distinct scenarios, specifically pertaining to the backward and forward expected losses: (1) **Strong Convexity and Lipschitz Smoothness Case.** We explore the convergence behavior when the losses exhibit both strong convexity and Lipschitz smoothness properties. (2) **Lipschitz Smoothness Case.** We investigate convergence when the losses are solely Lipschitz-smooth. Through a rigorous examination of these cases, we thus intend to provide a comprehensive understanding of the convergence characteristics of FB-MOAC algorithm.

We also need to emphasize that stochastic nature of FB-MDP affects the values of $\boldsymbol{\phi}$, $\boldsymbol{\psi}$ and $\boldsymbol{\theta}$, based on the SGD rules (Equations (13) and (15)), so they are treated as random variables.

We now make the following assumptions.

Assumption 1: The forward and bidirectional state-value functions are unbiased:

$$\mathbb{E}_{\boldsymbol{\phi}}\{V^f_{\boldsymbol{\phi},j}(\mathbf{s})\} = V^f_j(\mathbf{s}), \quad j \in S_f, \quad \mathbf{s} \in \mathcal{S}$$
$$\mathbb{E}_{\boldsymbol{\psi}}\{V^b_{\boldsymbol{\psi},j}(\mathbf{y},\mathbf{s})\} = V^b_j(\mathbf{y},\mathbf{s}), \quad j \in S_b, \quad (\mathbf{y},\mathbf{s}) \in \mathcal{Y}\times\mathcal{S},$$

According to this assumption and Equations (14) and (18) we can get:

$$\nabla_{\boldsymbol{\theta}}\bar{J}^f_j(\boldsymbol{\theta}) = \mathbb{E}_{\boldsymbol{\phi}}\,\mathbb{E}\left\{\nabla_{\boldsymbol{\theta}}\hat{J}^f_j(\boldsymbol{\theta},\boldsymbol{\phi}) \,\middle|\, \boldsymbol{\theta},\boldsymbol{\phi}\right\} = -\sum_{k=1}^{T}\mathbb{E}_{\boldsymbol{\phi}}\,\mathbb{E}\left\{\nabla_{\boldsymbol{\theta}}\log\pi_{\boldsymbol{\theta}}(\mathbf{a}_k|\mathbf{s}_k)A^f_{\boldsymbol{\phi},j}(\mathbf{s}_k,\mathbf{a}_k) \,\middle|\, \boldsymbol{\theta}\right\}$$
$$= -\mathbb{E}\left\{\sum_{k=1}^{T}\nabla_{\boldsymbol{\theta}}\log\pi_{\boldsymbol{\theta}}(\mathbf{a}_k|\mathbf{s}_k)A^f_j(\mathbf{s}_k,\mathbf{a}_k) \,\middle|\, \boldsymbol{\theta}\right\} = \nabla_{\boldsymbol{\theta}}J^f_j(\boldsymbol{\theta})$$

Likewise, it can be shown that:

$$\nabla_{\boldsymbol{\theta}}\bar{J}^b_j(\boldsymbol{\theta}) = -\mathbb{E}\left\{\sum_{k=1}^{T}\nabla_{\boldsymbol{\theta}}\log\pi_{\boldsymbol{\theta}}(\mathbf{a}_k|\mathbf{s}_k)A^b_j(\mathbf{y}_k,\mathbf{s}_k,\mathbf{a}_k) \,\middle|\, \boldsymbol{\theta}\right\} = \nabla_{\boldsymbol{\theta}}J^b_j(\boldsymbol{\theta})$$

Assumption 2.1: The forward and backward multi-objective expected losses are differentiable and strongly convex with parameters γ_f and γ_b, respectively, w.r.t $\boldsymbol{\theta}$:

$$\nabla^2_{\boldsymbol{\theta}}J^f_j(\boldsymbol{\theta}) - \gamma_f\boldsymbol{I} \succeq \mathbf{0}, \qquad j \in S_f$$
$$\nabla^2_{\boldsymbol{\theta}}J^b_j(\boldsymbol{\theta}) - \gamma_b\boldsymbol{I} \succeq \mathbf{0}, \qquad j \in S_b.$$

Assumption 2.2: The forward and backward multi-objective expected losses are differentiable and Lipschitz smooth functions with constants L_f and L_b, respectively, w.r.t $\boldsymbol{\theta}$:

$$\left\|\nabla_{\boldsymbol{\theta}}J^f_j(\boldsymbol{\theta}') - \nabla_{\boldsymbol{\theta}}J^f_j(\boldsymbol{\theta})\right\| \le L_f\|\boldsymbol{\theta}'-\boldsymbol{\theta}\|, \qquad j \in S_f.$$
$$\left\|\nabla_{\boldsymbol{\theta}}J^b_j(\boldsymbol{\theta}') - \nabla_{\boldsymbol{\theta}}J^b_j(\boldsymbol{\theta})\right\| \le L_b\|\boldsymbol{\theta}'-\boldsymbol{\theta}\|, \qquad j \in S_b.$$

Notice that the assumptions above are made for the expected losses ($J^f_j(\boldsymbol{\theta})$, $J^b_j(\boldsymbol{\theta})$) and not for the stochastic losses ($\hat{J}^f_j(\boldsymbol{\theta},\boldsymbol{\phi})$, $\hat{J}^b_j(\boldsymbol{\theta},\boldsymbol{\psi})$).

Assumption 3: Consider the following stochastic forward / backward gradient:

$$\nabla\hat{\boldsymbol{J}}^{\text{fb}}(\boldsymbol{\theta},\boldsymbol{\phi},\boldsymbol{\psi}) = \Big[\big[\nabla_{\boldsymbol{\theta}}\hat{J}^f_j(\boldsymbol{\theta},\boldsymbol{\phi})\big]_{j\in S_f}, \big[\nabla_{\boldsymbol{\theta}}\hat{J}^b_j(\boldsymbol{\theta},\boldsymbol{\psi})\big]_{j\in S_b}\Big],$$

then, its conditional covariance is bounded by a positive semi-definite matrix $\boldsymbol{B}$:

$$\mathbb{E}\left\{\nabla\hat{\boldsymbol{J}}^{\text{fb}}(\boldsymbol{\theta},\boldsymbol{\phi},\boldsymbol{\psi})^\top\nabla\hat{\boldsymbol{J}}^{\text{fb}}(\boldsymbol{\theta},\boldsymbol{\phi},\boldsymbol{\psi})\mid\boldsymbol{\theta}\right\}-\nabla\boldsymbol{J}^{\text{fb}}(\boldsymbol{\theta})^\top\nabla\boldsymbol{J}^{\text{fb}}(\boldsymbol{\theta})\preceq\boldsymbol{B},$$

where

$$\nabla\boldsymbol{J}^{\text{fb}}(\boldsymbol{\theta})(\boldsymbol{\theta},\boldsymbol{\phi},\boldsymbol{\psi})=\Big[\big[\nabla_{\boldsymbol{\theta}}j^f(\boldsymbol{\theta})\big]_{j\in S_f},\big[\nabla_{\boldsymbol{\theta}}J_j^b(\boldsymbol{\theta})\big]_{j\in S_b}\Big],$$

Note that the assumptions outlined in this context align with the conventions found in the literature related to convergence analysis (Qiu et al., 2021; Zhou et al., 2022).

Now, we have the following theorem.

Theorem B.1. *Consider forward / backward expected losses, i.e., $\{J_j^f(\cdot)\}_{j\in S_f}$ and $\{J_j^b(\cdot)\}_{j\in S_b}$, and forward / backward stochastic losses, i.e., $\{\hat{J}_j^f(\cdot,\cdot)\}_{j\in S_f}$ and $\{\hat{J}_j^b(\cdot,\cdot)\}_{j\in S_b}$, complying with Assumptions 2.1, 2.2 and 3, and $\boldsymbol{\beta}_{\text{act}}$ being the solution of Equation* (16)*. Moreover, consider SGDes in Equations* (12) *and* (15) *characterized by iteration number i and actor learning rate $\{\mu_i\}_{i\in\mathcal{I}}$ with*

$$\mu_i\leq\min\left\{\frac{1}{\max\{L_f,L_b\}},\frac{1}{\max\{L_f,L_b\}\|\mathbf{B}\|}\mathbb{E}\Big\{\frac{1}{\mathbf{1}^\top\left(\nabla\boldsymbol{J}^{\text{fb}}(\boldsymbol{\theta}^i)^\top\nabla\boldsymbol{J}^{\text{fb}}(\boldsymbol{\theta}^i)\right)^{-1}\mathbf{1}}\Big\}\right\},$$

which generate sequences $\{\boldsymbol{\phi}^i\}_{i\in\mathcal{I}}$, $\{\boldsymbol{\psi}^i\}_{i\in\mathcal{I}}$ and $\{\boldsymbol{\theta}^i\}_{i\in\mathcal{I}}$, we then get:

$$\mathbb{E}\,J_j^f(\boldsymbol{\theta}^{i+1})\;\leq\;\mathbb{E}\,J_j^f(\boldsymbol{\theta}^i),\qquad j\in S_f$$

and

$$\mathbb{E}\,J_j^b(\boldsymbol{\theta}^{i+1})\;\leq\;\mathbb{E}\,J_j^b(\boldsymbol{\theta}^i),\qquad j\in S_b.$$

Proof. According to the update rule Equation (15), we have:

$$\boldsymbol{\theta}^{i+1}=\boldsymbol{\theta}^i-\mu_i\big[\nabla\hat{\boldsymbol{J}}^{\text{f}}(\boldsymbol{\theta}^i,\boldsymbol{\phi}^i),\nabla\hat{\boldsymbol{J}}^{\text{b}}(\boldsymbol{\theta}^i,\boldsymbol{\psi}^i)\big]\boldsymbol{\beta}_{\text{act}}^i=\boldsymbol{\theta}^i-\mu_i\nabla\hat{\boldsymbol{J}}^{\text{fb}}(\boldsymbol{\theta}^i,\boldsymbol{\phi}^i,\boldsymbol{\psi}^i)\boldsymbol{\beta}_{\text{act}}^i.$$

Based on Assumption 2.2, we then obtain:

$$J_j^f(\boldsymbol{\theta}^{i+1})-J_j^f(\boldsymbol{\theta}^i)\leq-\mu_i\nabla J_j^f(\boldsymbol{\theta}^i)^\top\nabla\hat{\boldsymbol{J}}^{\text{fb}}(\boldsymbol{\theta}^i,\boldsymbol{\phi}^i,\boldsymbol{\psi}^i)\boldsymbol{\beta}_{\text{act}}^i+\frac{\mu_i^2L_f}{2}{\boldsymbol{\beta}_{\text{act}}^i}^\top\nabla\hat{\boldsymbol{J}}^{\text{fb}}(\boldsymbol{\theta}^i,\boldsymbol{\phi}^i,\boldsymbol{\psi}^i)^\top\nabla\hat{\boldsymbol{J}}^{\text{fb}}(\boldsymbol{\theta}^i,\boldsymbol{\phi}^i,\boldsymbol{\psi}^i)\boldsymbol{\beta}_{\text{act}}^i.$$

By taking the expectation on both sides of the recent equation, it then reads:

$$\mathbb{E}\Big\{J_j^f(\boldsymbol{\theta}^{i+1})-J_j^f(\boldsymbol{\theta}^i)\Big\}\leq-\mu_i\mathbb{E}\Big\{\Big(\boldsymbol{e}_j-\frac{\mu_iL_f}{2}\boldsymbol{\beta}_{\text{act}}^i\Big)^\top\nabla\boldsymbol{J}^{\text{fb}}(\boldsymbol{\theta}^i)^\top\nabla\boldsymbol{J}^{\text{fb}}(\boldsymbol{\theta}^i)\boldsymbol{\beta}_{\text{act}}^i\Big\}+\frac{\mu_i^2L_f}{2}\|\boldsymbol{B}\|,\tag{28}$$

where was obtained based on

$$\mathbb{E}_{\boldsymbol{\phi}^i,\boldsymbol{\psi}^i}\,\mathbb{E}\left\{{\boldsymbol{\beta}_{\text{act}}^i}^\top\nabla\boldsymbol{J}^f(\boldsymbol{\theta}^i)^\top\nabla\hat{\boldsymbol{J}}^{\text{fb}}(\boldsymbol{\theta}^i,\boldsymbol{\phi}^i,\boldsymbol{\psi}^i)\boldsymbol{\beta}_{\text{act}}^i\mid\boldsymbol{\theta}^i,\boldsymbol{\phi}^i,\boldsymbol{\psi}^i\right\}={\boldsymbol{\beta}_{\text{act}}^i}^\top\nabla\boldsymbol{J}^f(\boldsymbol{\theta}^i)^\top\nabla\boldsymbol{J}^{\text{fb}}(\boldsymbol{\theta}^i)\boldsymbol{\beta}_{\text{act}}^i$$

according to Assumption 1, as well as based on Assumption 3 and ${\boldsymbol{\beta}_{\text{act}}^i}^\top\boldsymbol{B}\boldsymbol{\beta}_{\text{act}}^i\leq\|\boldsymbol{B}\|\,\|\boldsymbol{\beta}_{\text{act}}^i\|^2\leq\|\boldsymbol{B}\|$. On the other hand, from Equation (16), for all $\beta_{\text{act,j}}^i\geq0$, it reads:

$$\boldsymbol{\beta}_{\text{act}}^i=\left(\mathbf{1}^\top\left(\nabla\boldsymbol{J}^{\text{fb}}(\boldsymbol{\theta}^i)^\top\nabla\boldsymbol{J}^{\text{fb}}(\boldsymbol{\theta}^i)\right)^{-1}\mathbf{1}\right)^{-1}\left(\nabla\boldsymbol{J}^{\text{fb}}(\boldsymbol{\theta}^i)^\top\nabla\boldsymbol{J}^{\text{fb}}(\boldsymbol{\theta}^i)\right)^{-1}\mathbf{1}.$$

By substituting this into Equation (28), we get:

$$\mathbb{E}\Big\{J_j^f(\boldsymbol{\theta}^{i+1})-J_j^f(\boldsymbol{\theta}^i)\Big\}\overset{a}{\leq}-\frac{\mu_i}{2}\mathbb{E}\left\{\frac{1}{\mathbf{1}^\top\left(\nabla\boldsymbol{J}^{\text{fb}}(\boldsymbol{\theta}^i)^\top\nabla\boldsymbol{J}^{\text{fb}}(\boldsymbol{\theta}^i)\right)^{-1}\mathbf{1}}\right\}+\frac{\mu_i^2L_f}{2}\|\boldsymbol{B}\|\;\leq\;0,$$

where we used $\mu_i \max\{L_f, L_b\} \leq 1$ for (a). Considering that the denominator of RHS of the recent equation is positive due to the positive-definiteness of $\left(\nabla \boldsymbol{J}^{\text{fb}}(\boldsymbol{\theta}^i)^\top \nabla \boldsymbol{J}^{\text{fb}}(\boldsymbol{\theta}^i)\right)^{-1}$, the statement follows. The same analysis can be applied to infer $\mathbb{E}\Big\{ J_j^b(\boldsymbol{\theta}^{i+1}) - J_j^b(\boldsymbol{\theta}^i) \Big\} \leq 0$ □

Remark B.2. Theorem B.1 guarantees all the forward and backward expected losses $\left\{\mathbb{E}\, J_j^f(\boldsymbol{\theta})\right\}_{j\in S_f}$ and $\left\{\mathbb{E}\, J_j^b(\boldsymbol{\theta})\right\}_{j\in S_b}$ continually reduce as the algorithm iteration increases. It thus enables us to jointly improve all of the cumulative rewards, either forward or backward, with each iteration, on average.

Corollary B.3. *Consider the framework of Lemma B.1, we then get:*

$$\mathbb{E}\left\{ {\boldsymbol{\beta}_{\text{act}}^i}^\top \nabla \boldsymbol{J}^{\text{fb}}(\boldsymbol{\theta}^i)^\top \nabla \boldsymbol{J}^{\text{fb}}(\boldsymbol{\theta}^i) \boldsymbol{\beta}_{\text{act}}^i \right\} \leq \frac{2}{\mu_i} \mathbb{E}\left\{ \sum_{j\in S_f \cup S_b} \beta_{\text{act,j}}^i \left(J_j^{\text{fb}}(\boldsymbol{\theta}^i) - J_j^{\text{fb}}(\boldsymbol{\theta}^{i+1}) \right) \right\} + \mu_i \max\{L_f, L_b\} \|\boldsymbol{B}\|.$$

Proof. Based on Equation (28) and $\mu_i \max\{L_f, L_b\} \leq 1$, the statement follows. □

B.1 Analysis for Strongly-convex and Lipschitz-smooth Losses

Theorem B.4. *Consider the framework of Theorem B.1, and assume forward-backward multi-objective optimization O_2 with a $\boldsymbol{\theta}$-parametric policy distribution $\pi_{\boldsymbol{\theta}}(\cdot|\cdot)$ being optimized by the SGDs in Equations* (13) *and* (15) *with generated sequences $\{\boldsymbol{\theta}^i\}_{i\in\mathcal{I}}$, $\{\boldsymbol{\phi}^i\}_{i\in\mathcal{I}}$ and $\{\boldsymbol{\psi}^i\}_{i\in\mathcal{I}}$, and actor learning rate $\{\mu_i\}_{i\in\mathcal{I}}$ complying with assumptions of Theorem B.1. Furthermore, assume there exists a Pareto-optimal solution $\boldsymbol{\theta}^*$ of O_2 dominating $\boldsymbol{\theta}^i$ for the objectives $\{J_j^{\text{fb}}(\cdot)\}_{j\in S_f\cup S_b}$ with $i \in \mathcal{I}$. Then, we have:*

$$\mathbb{E}\|\boldsymbol{\theta}^{i+1} - \boldsymbol{\theta}^*\| \leq \big(1 - \max\{\gamma_f, \gamma_b\}\mu_i\big)\, \mathbb{E}\|\boldsymbol{\theta}^i - \boldsymbol{\theta}^*\| + \big(1 + \max\{L_f, L_b\}\big)\mu_i^2 \|\boldsymbol{B}\|. \tag{29}$$

Proof. Based on the SGD update in Equation (15), we obtain:

$$\begin{aligned}
\mathbb{E}\|\boldsymbol{\theta}^{i+1} - \boldsymbol{\theta}^*\|^2 &= \mathbb{E}\|\boldsymbol{\theta}^i - \boldsymbol{\theta}^* - \mu_i \nabla \hat{\boldsymbol{J}}^{\text{fb}}(\boldsymbol{\theta}^i, \boldsymbol{\phi}^i, \boldsymbol{\psi}^i)\boldsymbol{\beta}_{\text{act}}^i\|^2 \leq\ \mathbb{E}\|\boldsymbol{\theta}^i - \boldsymbol{\theta}^*\|^2 \\
&\quad - 2\mu_i \mathbb{E}\Big\{ \mathbb{E}\Big\{ \sum_{j\in S_f\cup S_b} \beta_{\text{act,j}}^i \nabla \hat{J}_j^{\text{fb}}(\boldsymbol{\theta}^i, \boldsymbol{\phi}^i, \boldsymbol{\psi}^i)^\top \big(\boldsymbol{\theta}^i - \boldsymbol{\theta}^*\big) \;\big|\; \boldsymbol{\theta}^i, \boldsymbol{\phi}^i, \boldsymbol{\psi}^i \Big\} \Big\} \\
&\quad + \mathbb{E}\left\{ {\boldsymbol{\beta}_{\text{act}}^i}^\top \nabla \hat{\boldsymbol{J}}^{\text{fb}}(\boldsymbol{\theta}^i, \boldsymbol{\phi}^i, \boldsymbol{\psi}^i)^\top \nabla \hat{\boldsymbol{J}}^{\text{fb}}(\boldsymbol{\theta}^i, \boldsymbol{\phi}^i, \boldsymbol{\psi}^i) \boldsymbol{\beta}_{\text{act}}^i \right\} \\
&\overset{a}{\leq} \mathbb{E}\|\boldsymbol{\theta}^i - \boldsymbol{\theta}^*\|^2 - 2\mu_i \mathbb{E}\Big\{ \sum_{j\in S_f\cup S_b} \beta_{\text{act,j}}^i \nabla J_j^{\text{fb}}(\boldsymbol{\theta}^i)^\top \big(\boldsymbol{\theta}^i - \boldsymbol{\theta}^*\big) \Big\} \\
&\quad + \mathbb{E}\left\{ {\boldsymbol{\beta}_{\text{act}}^i}^\top \nabla \hat{\boldsymbol{J}}^{\text{fb}}(\boldsymbol{\theta}^i, \boldsymbol{\phi}^i, \boldsymbol{\psi}^i)^\top \nabla \hat{\boldsymbol{J}}^{\text{fb}}(\boldsymbol{\theta}^i, \boldsymbol{\phi}^i, \boldsymbol{\psi}^i) \boldsymbol{\beta}_{\text{act}}^i \right\} \\
&\overset{b}{\leq} \big(1 - \max\{\gamma_f, \gamma_b\}\mu_i\big)\, \mathbb{E}\|\boldsymbol{\theta}^i - \boldsymbol{\theta}^*\|^2 + 2\mu_i \mathbb{E}\Big\{ \sum_{j\in S_f\cup S_b} \beta_{\text{act,j}}^i \big(J_j^{\text{fb}}(\boldsymbol{\theta}^*) - J_j^{\text{fb}}(\boldsymbol{\theta}^i) \big) \Big\} \\
&\quad + \mu_i^2 \mathbb{E}\left\{ \mathbb{E}\Big\{ {\boldsymbol{\beta}_{\text{act}}^i}^\top \nabla \hat{\boldsymbol{J}}^{\text{fb}}(\boldsymbol{\theta}^i, \boldsymbol{\phi}^i, \boldsymbol{\psi}^i)^\top \nabla \hat{\boldsymbol{J}}^{\text{fb}}(\boldsymbol{\theta}^i, \boldsymbol{\phi}^i, \boldsymbol{\psi}^i) \boldsymbol{\beta}_{\text{act}}^i \;\big|\; \boldsymbol{\theta}^i, \boldsymbol{\phi}^i, \boldsymbol{\psi}^i \Big\} \right\} \\
&\overset{c}{\leq} \big(1 - \max\{\gamma_f, \gamma_b\}\mu_i\big) \mathbb{E}\|\boldsymbol{\theta}^i - \boldsymbol{\theta}^*\|^2 + \mu_i^2 \|\boldsymbol{B}\| + 2\mu_i \mathbb{E}\Big\{ \sum_{j\in S_f\cup S_b} \beta_{\text{act,j}}^i \Big(J_j^{\text{fb}}(\boldsymbol{\theta}^*) - J_j^{\text{fb}}(\boldsymbol{\theta}^{i+1}) \Big) \Big\} \\
&\overset{d}{\leq} \big(1 - \max\{\gamma_f, \gamma_b\}\mu_i\big)\, \mathbb{E}\|\boldsymbol{\theta}^i - \boldsymbol{\theta}^*\|^2 + \big(1 + \max\{L_f, L_b\}\big)\mu_i^2 \|\boldsymbol{B}\|,
\end{aligned}$$

where (a) was achieved considering $\mathbb{E}_{\boldsymbol{\phi},\boldsymbol{\psi}}\mathbb{E}\{\nabla \hat{\boldsymbol{J}}^{\text{fb}}(\boldsymbol{\theta}, \boldsymbol{\phi}, \boldsymbol{\psi}) | \boldsymbol{\theta}, \boldsymbol{\phi}, \boldsymbol{\psi}\} = \nabla \boldsymbol{J}^{\text{fb}}(\boldsymbol{\theta})$ based on Assumption 1, (b) was obtained based on Assumption 2.1, (c) according to Assumption 3 and Corollary B.3, and for (d) we exploited $\boldsymbol{\theta}^*$ being a dominating Pareto optimum. □

Accordingly, we can obtain the following corollary.

Corollary B.5. *Consider the SGD approach in Equation* (15) *with generated sequence* $\{\boldsymbol{\theta}^n\}_{n\in\mathcal{I}}$ *and actor learning rate* $\{\mu_n\}_{n\in\mathcal{I}}$ *complying with assumptions of Theorem B.1. Set* μ_n *so that* $\lim_{n\to\infty}\mu_n = 0$*, then* $\lim_{n\to\infty}\mathbb{E}\|\boldsymbol{\theta}^n - \boldsymbol{\theta}^*\|^2 = 0$*, where* $\boldsymbol{\theta}^*$ *is a Pareto-optimal solution of* O_2*.*

Proof. We use the result provided in Turinici (2021). As such, based on Theorem B.4 we have:

$$\begin{aligned}\Delta_{n+1} - \epsilon \;&\leq\; \big(1 - \max\{\gamma_f, \gamma_b\}\mu_n\big)(\Delta_n - \epsilon) - \mu_n\big(\max\{\gamma_f, \gamma_b\}\epsilon - (1 + \max\{L_f, L_b\})\mu_n\|\boldsymbol{B}\|\big)\\ &\overset{a}{\leq}\; \big(1 - \max\{\gamma_f, \gamma_b\}\mu_n\big)(\Delta_n - \epsilon).\end{aligned}$$

where $\Delta_n = \mathbb{E}\|\boldsymbol{\theta}^n - \boldsymbol{\theta}^*\|^2$ and $\epsilon > 0$. For (a), we considered $\max\{\gamma_f, \gamma_b\}\epsilon - \big(1 + \max\{L_f, L_b\}\big)\mu_n\|\boldsymbol{B}\| \geq 0$ for a large n. Hence, for $\max\{\gamma_f, \gamma_b\}\mu_n \leq 1$ it reads:

$$[\Delta_{n+1} - \epsilon]^+ \leq \big(1 - \max\{\gamma_f, \gamma_b\}\mu_n\big)[\Delta_n - \epsilon]^+,$$

where $[x]^+ = x + |x|$. By iterating, we get:

$$[\Delta_{n+k} - \epsilon]^+ \leq \prod_{i=0}^{k-1}\big(1 - \max\{\gamma_f, \gamma_b\}\mu_{n+i}\big)\,[\Delta_n - \epsilon]^+.$$

Considering that $\lim_{k\to\infty}\prod_{i=0}^{k-1}\big(1 - \max\{\gamma_f, \gamma_b\}\mu_{n+i}\big) = 0$, we have: $\lim_{m\to\infty}[\Delta_m - \epsilon]^+$. The statement follows as the previous expression holds for any value $\epsilon > 0$. □

Remark B.6. The results of Theorem B.4 and Corollary B.5 guarantees that a convergence-in-mean towards a Pareto-optimal solution can be achieved by choosing a suitable actor learning rate. More specifically, a convergence-in-mean with the rate of $\mathcal{O}(1/|\mathcal{I}|)$ can be achieved for the learning rate being set to $\mu_i = \mathcal{O}(1/i)$.

Remark B.7. The result of Corollary B.5 can be verified in a distinct quantitative way. More specifically, for the learning rate μ_i being sufficiently small, the evolution of the SGD Equation (15) can be regarded in a continuous time flow with parameter t. As such, based on 29, the dynamics of $\Delta_i = \mathbb{E}\|\boldsymbol{\theta}^i - \boldsymbol{\theta}^*\|$ can be expressed by the following inequality:

$$\Delta_\tau \leq \Delta_0\,\exp\Big(-\max\{\gamma_f, \gamma_b\}\int_0^\tau \mu_s ds\Big) + \big(1 + \max\{L_f, L_b\}\big)\|\mathbf{B}\|\int_0^\tau \mu_t^2\,\exp\Big(-\max\{\gamma_f, \gamma_b\}\int_t^\tau \mu_s ds\Big)dt.$$

Thus, the selection $\mu_t = \frac{c_0}{t}$ allows to get $\lim_{\tau\to\infty}\Delta_\tau \to 0$ by yielding:

$$\lim_{i\to\infty}\mathbb{E}\|\boldsymbol{\theta}^i - \boldsymbol{\theta}^*\| \to 0.$$

B.2 Analysis for Lipschitz-smooth Losses

Assuming strong-convexity for the expected losses may not be a reasonable assumption, particularly when the NN architecture of the actor agent exhibits non-linearity. Motivated by this fact, we perform a convergence analysis without imposing the strong-convexity assumption, focusing solely on the smoothness condition as defined in Assumption 2.2. In light of this approach, we thus have the following theorem.

Theorem B.8. *Consider forward / backward expected losses, i.e.,* $\{J_j^f(\cdot)\}_{j\in S_f}$ *and* $\{J_j^b(\cdot)\}_{j\in S_b}$*, and forward / backward stochastic losses, i.e.,* $\{\hat{J}_j^f(\cdot,\cdot)\}_{j\in S_f}$ *and* $\{\hat{J}_j^b(\cdot,\cdot)\}_{j\in S_b}$*, complying with Assumptions 2.2 and 4, and* $\boldsymbol{\beta}_{\text{act}}$ *being the solution of Equation* (16)*. Moreover, consider SGDs in Equations* (12) *and* (15) *characterized by iteration number* i *and actor learning rate* $\{\mu_i\}_{i\in\mathcal{I}}$ *with*

$$\mu_i \leq \min\left\{\frac{1}{\max\{L_f, L_b\}}, \frac{1}{\max\{L_f, L_b\}\|\boldsymbol{B}\|}\left(\mathbf{1}^\top\left(\nabla\boldsymbol{J}^{\text{fb}}(\boldsymbol{\theta}^i)^\top\nabla\boldsymbol{J}^{\text{fb}}(\boldsymbol{\theta}^i)\right)^{-1}\mathbf{1}\right)^{-1}\right\},$$

and $0 < \mu_{|\mathcal{I}|} \leq \ldots \leq \mu_i \leq \ldots \leq \mu_1$*, which generate sequences* $\{\boldsymbol{\phi}^i\}_{i\in\mathcal{I}}$*,* $\{\boldsymbol{\psi}^i\}_{i\in\mathcal{I}}$ *and* $\{\boldsymbol{\theta}^i\}_{i\in\mathcal{I}}$*. Then, we get:*

$$\begin{aligned}\min_{i\in\mathcal{I}}\mathbb{E}\Big\{\|\nabla\boldsymbol{J}^{\text{fb}}(\boldsymbol{\theta}^i)\boldsymbol{\beta}_{\text{act}}^i\|^2\Big\} \leq\; &\frac{\max\{L_f, L_b\}\,\|\boldsymbol{B}\|}{|\mathcal{I}|}\sum_{i\in\mathcal{I}}\frac{\mu_i}{2 - \mu_i\max\{L_f, L_b\}}\\ &+ \frac{2}{|\mathcal{I}|\,\mu_{|\mathcal{I}|}}\sum_{j\in S_f\cup S_b}\mathbb{E}\big\{J_j^{\text{fb}}(\boldsymbol{\theta}^1) - J_j^{\text{fb}}(\boldsymbol{\theta}^{|\mathcal{I}|})\big\}.\end{aligned} \tag{30}$$

where $\boldsymbol{J}^{\text{fb}}(\boldsymbol{\theta}) = \Big[\big[J_j^f(\boldsymbol{\theta})\big]_{j\in S_f}, \big[J_j^b(\boldsymbol{\theta})\big]_{j\in S_b}\Big]$.

Proof. Based on Equation (28), we can get:

$$\sum_{j\in S_f\cup S_b} \beta_{\text{ac,j}}^i\big(J_j^{\text{fb}}(\boldsymbol{\theta}^{i+1}) - J_j^{\text{fb}}(\boldsymbol{\theta}^i)\big) \leq \mu_i\big(\frac{\mu_i}{2}\max\{L_f, L_b\} - 1\big)\boldsymbol{\beta}_{\text{act}}^{i\,\top}\nabla\boldsymbol{J}^{\text{fb}}(\boldsymbol{\theta}^i)^\top\nabla\boldsymbol{J}^{\text{fb}}(\boldsymbol{\theta}^i)\boldsymbol{\beta}_{\text{act}}^i + \frac{\mu_i^2}{2}\max\{L_f, L_b\}\|\boldsymbol{B}\|.$$

Therefore, we have:

$$\mathbb{E}\Big\{\|\nabla\boldsymbol{J}^{\text{fb}}(\boldsymbol{\theta}^i)\boldsymbol{\beta}_{\text{ac}}^i\|^2\Big\} \leq \frac{1}{\mu_i(1-\frac{\mu_i}{2}\max\{L_f, L_b\})}\,\mathbb{E}\Big\{\sum_{j\in S_f\cup S_b}\beta_{\text{act,j}}^i\big(J_j^{\text{fb}}(\boldsymbol{\theta}^i) - J_j^{\text{fb}}(\boldsymbol{\theta}^{i+1})\big)\Big\} + \frac{\mu_i\max\{L_f, L_b\}}{2-\mu_i\max\{L_f, L_b\}}\|\boldsymbol{B}\|.$$

the statement follows by using the result of Theorem B.1, $\beta_{\text{act,j}} \leq 1$ for $j \in S_f \cup S_b$ and applying telescopic cancellation. □

Remark B.9. Note that the result of Theorem B.8 implies the convergence to a locally Pareto-optimal solution (Zhou et al., 2022) provided that a suitable dynamics for the learning rate is chosen. Specifically, it shows a convergence rate of $\mathcal{O}(1/\sqrt{|\mathcal{I}|})$ when the learning rate is set to $\mu_i = \mathcal{O}(1/\sqrt{i})$.

Remark B.10. Notice that the selection $\mu_i = \mathcal{O}(1/i)$ cannot lead to a convergence due to the second term in the RHS of Equation (30). This is contrast to the findings in Section B.1, where a convergence rate of $\mathcal{O}(1/|\mathcal{I}|)$ can be achieved for the strongly-convex and Lipschitz smooth case.

C Additional Details on the Edge Caching Use Case

The environment of this experiment is a cellular network with cache-equipped Base-Stations (BSs) similar to that in (Amidzadeh et al., 2023). The BSs are spatially distributed across the network with intensities λ_{bs}. The environment also includes a library containing N different contents as well as fixed mobile users requesting them from the cellular network. The network operates over time slots with index $t \in \{1, \ldots, T\}$, where T is the total duration of the operation. The network thus addresses that user requests in the beginning of each time slot. Contents have different *popularity* $\{p_n^{\text{pop}}(t)\}_{n=1}^N$, where $p_n^{\text{pop}}(t)$ is the probability that content n is requested by a randomly selected user at time t. The goal is to satisfy as many users as possible during the network operation. At the beginning of each time-slot, the BSs cache the most popular contents with probability $\{p_n^{\text{cach}}(t)\}_{n=1}^N$ and simultaneously *multicast* them toward users by consuming content-specific radio resources $\{w_n(t)\}_{n=1}^N$. We denote the system action parameters by the vector $\mathbf{a}(t)$, which depends on the content-specific bandwidth allocation and cache placement of BSs, i.e., $\mathbf{a}(t) = [\{p_n^{\text{cach}}(t)\}_{n=1}^N, \{w_n(t)\}_{n=1}^N]$. A multicast outage may occur with probability $\{O_n(\mathbf{a}(t), t)\}_{n=1}^N$:

$$O_n(\mathbf{a}(t), t) = \text{erfc}\left(\frac{\pi^2\lambda_{bs}p_n^{\text{cach}}(t)}{4\sqrt{\eta_n(t)}}\right), \quad \eta_n(t) = 2^{1/w_n(t)} - 1, \tag{31}$$

where obtained by averaging over users. As a result, certain users fail to receive the requested content in the current timeslot and their request is deferred to the subsequent one. Hence, each time-slot sees a distribution of users accounting for the repeated requests and a distribution describing the new preferences toward contents. This leads to a time-varying model for the request probability of content n, $p_n^{\text{req}}(t)$:

$$p_n^{\text{req}}(t) = \underbrace{p_n^{\text{req}}(t-1)O_n\big(\mathbf{a}(t-1), t-1\big)}_{\text{repeated request}} + \underbrace{p_n^{\text{pop}}(t)\sum_{m=1}^N\big(1 - O_m\big(\mathbf{a}(t-1), t-1\big)\big)p_m^{\text{req}}(t-1)}_{\text{new request based on the popularity}}. \tag{32}$$

Note that $p_n^{\mathrm{req}}(t)$ indicates the request probability of content n averaged over all users. Then, it can be simply verified that $\sum_{n=1}^{N} p_n^{\mathrm{req}}(t) = 1$, considering $\sum_{n=1}^{N} p_n^{\mathrm{pop}}(t) = 1$. Equation (32) therefore represents a **forward dynamics**, with the forward state vector $\mathbf{s}(t) = \mathbf{p}^{\mathrm{req}}(t)$ and the action vector $\mathbf{a}(t)$.

A request for a content is repeated across several time-slots until successfully fulfilled, resulting in an expected latency $L_n(t)$ for successful delivery of content n. For this quantity, a time-varying dynamics can be derived by the law of total expectation as follows:

$$\begin{aligned} L_n(\mathbf{a}(t), t) &= \mathbb{E}\{\text{latency} \mid \text{outage}\}\mathbb{P}\{\text{outage}\} + \mathbb{E}\{\text{latency}\mid \text{no outage}\}\mathbb{P}\{\text{no outage}\} \\ &= \Big(d(t) + L_n(t+1)\Big) O_n(\mathbf{a}(t), t) + \frac{d(t)}{2}\big(1 - O_n(\mathbf{a}(t), t)\big), \end{aligned} \tag{33}$$

where $d(t)$ is the duration of time-slot t in seconds, and $L_n(\mathbf{a}(T), T) = 0$ since system operations finish and the users do not need to wait any longer. Equation (33) represents a **backward dynamics**, with the backward state vector $\mathbf{y}(t) = \mathbf{L}(t)$ and the action vector $\mathbf{a}(t)$. Note that this model fully captures the trade-offs involved in the delay dynamics and differs from the conventional formalism that does not provide a continuum model when accounting for successive slots; for the delivery without outage, the expected latency simply becomes $L_n(t) = \frac{d(t)}{2}$, as its realizations follow a uniform distribution with values between 0 and $d(t)$. Notice that the backward dynamics (33) based on Theorem 3.6 cannot be expressed as a standard MDP. Thus, Equations (32) and (33) together model a FB-MDP and are coupled through the action $\mathbf{a}(t)$. Hence, they should be jointly considered to obtain an optimal cache policy.

D Case Study: Computation Offloading

We now present an additional use case in the domain of computation offloading (Zabihi et al., 2023).

D.1 System Model

There are N_{dev} mobile devices and N computational intensive tasks with diverse sizes $\{s_n\}_{n=1}^{N}$. A typical mobile device prefers task n with probability $p_n^{\mathrm{prf}}(t)$, and it *offloads* the preferred tasks with probability $p_n^{\mathrm{off}|\mathrm{prf}}(t)$ to an edge server. The server operates in time slots with duration τ indexed by t and leverages a task-specific parallelism mechanism to process the offloaded tasks. Specifically, it employs N buffers and N computational resources with $B_n^{\mathrm{edg}}(t)$ denoting the buffer capacity and $C_n^{\mathrm{edg}}(t) \geq C_{\min}^{\mathrm{edg}}$ denoting the computational resource allocated to file n. $C_{\min}^{\mathrm{edg}}$ is the minimum extent of allocated resource, while $\sum_{n=1}^{N} B_n^{\mathrm{edg}}(t) = B^{\mathrm{edg}}$ and $\sum_{n=1}^{N} C_n^{\mathrm{edg}}(t) = C^{\mathrm{edg}}$ represent the total buffer limit B^{edg} and computational capacity C^{edg}, respectively. The control parameters for this problem are thus $\{(p_n^{\mathrm{off}|\mathrm{prf}}(\cdot), B_n^{\mathrm{edg}}(\cdot), C_n^{\mathrm{edg}}(\cdot))\}_{n=1}^{N}$. A typical device offloading task n encounters with a failure if the corresponding buffer overflows, and as such it needs to re-offload the task. The queue length for n-th buffer S_n thus complies with the following expression:

$$L_n(t+1) = \max\Big\{L_n(t) + \underbrace{S_n p_n^{\mathrm{off}}(t+1)\alpha_n(t+1)}_{\text{new data buffered}} - \underbrace{C_n^{\mathrm{edg}}(t+1)}_{\text{computed data de-buffered}}, 0\Big\}, \tag{34}$$

for $n \in \{1, \ldots, N\}$, where $S_n = s_n\, N_{\mathrm{dev}}$, $p_n^{\mathrm{off}}(t)$ is the offloading probability for file n, $S_n p_n^{\mathrm{off}}(t)$ shows the total amount of data offloaded for the n-th buffer, and

$$\alpha_n(t+1) = \min\Big\{\frac{B_n^{\mathrm{edg}}(t+1) - L_n(t)}{S_n p_n^{\mathrm{off}}(t+1)}, 1\Big\},$$

denotes the fraction of data that can be buffered due to the buffer capacity B_n^{edg}. Therefore, it can be simply verified that $L_n(t+1) \leq B_n^{\mathrm{edg}}(t+1)$. The overflow probability $\mathcal{O}_n$ for n-th buffer is thus obtained by $\mathcal{O}_n(t) = 1 - \alpha_n(t)$. This equation exhibits a controlled forward dynamics, based on which we constitute the forward state $[\mathbf{p}^{\mathrm{prf}}(t), \mathbf{L}(t)]$ for this dynamics.

We now compute the *average computation time* needed for a typical device preferring task n, i.e., $t_n^{\mathrm{prf}}(t)$. If the task is preferred and locally computed, $t_n^{\mathrm{prf}}(t)$ depends on the computation capacity of the device itself,

whereas if it is offloaded, $t_n^{\text{prf}}(t)$ depends on the computation offloading time $t_n^{\text{off}}(t)$, i.e., average computation time needed for a device to offload task n. By the law of total expectation we thus get:

$$t_n^{\text{prf}}(t) = \mathbb{E}\{\text{computation time} \mid \text{task preferred}\} = p_n^{\text{off}|\text{prf}}(t)\, t_n^{\text{off}}(t) + (1 - p_n^{\text{off}|\text{prf}}(t))\frac{s_n}{C^{\text{dev}}}. \tag{35}$$

We thus need to compute $t_n^{\text{off}}(t)$. If the task being offloaded faces with an overflow, it will be re-offloaded in the next time-slot. However, if no overflow happens the computation time depends on the queue length and the computation resource allocated to the task. Therefore, $t_n^{\text{off}}(t)$ is found by the total expectation law as follows:

$$t_n^{\text{off}}(t) = \mathbb{E}\{\text{computation time} \mid \text{task offloaded }\} = \mathcal{O}_n(t+1)(\tau + t_n^{\text{prf}}(t+1)) + (1 - \mathcal{O}_n(t+1))\, t_n, \tag{36}$$

for $n \in \{1, \ldots, N\}$, where t_n stands for the needed time to compute task n with size s_n if it is successfully buffered. We thus have:

$$t_n = \frac{L_n(t) + \frac{1}{2}\alpha_n(t+1)p_n^{\text{off}}(t+1)S_n + s_n}{C_n^{\text{edg}}(t+1)}\tau,$$

where obtained considering that n-th buffer has already a queue with length $L_n(t)$ and additionally buffer S_n with probability $\frac{1}{2}\alpha_n(t+1)p_n^{\text{off}}(t+1)$. Equations (35) and (36) together provide a continuum model for the average time required to successfully compute task n within different slots. Additionally, they represent a controlled backward dynamics with the backward state $\mathbf{t}^{\text{prf}}(t) = [t_1^{\text{prf}}, \ldots, t_n^{\text{prf}}](t)$. We now consider two action-coupled conflicting rewards. The forward reward is related to the overall overflow probability as:

$$r_{\text{OP}}(t) = -\sum_{n=1}^{N} p_n^{\text{prf}}(t)\mathcal{O}_n(t),$$

and the backward reward is related to the expected computation time:

$$r_{\text{CT}}(t) = -\sum_{n=1}^{N} p_n^{\text{prf}}(t)t_n^{\text{prf}}(t),$$

This problem thus represents a FB-MDP environment with action $\left[\{C_n^{\text{edg}}\}_n, \{B_n^{\text{edg}}\}_n, \{p_n^{\text{off}|\text{prf}}\}_n\right]$, and action space $[0,1]^N \times [0,1]^N \times [0,1]^N$.

D.2 Experiment Setup and Hyper-parameters

We set the number of devices to $N_{\text{dev}} = 100$, number of tasks $N = 20$, file size $s_n = 10 + n$ Kbits, devices computational capacity $C^{\text{dev}} = 10$ Kbits/slot, minimum extent of allocated resource $C_{\text{min}}^{\text{edg}} = 10^{-5}$, edge computational capacity $C^{\text{edg}} = 100$ Kbits/slot edge buffer capacity $B = 100$ Kbits and slot duration $\tau = 60$ seconds. The hyper-parameters of FB-MOAC are the same as the previous experiment excluding the learning rates of actors and critics, which are set to 3×10^{-3}.

D.3 Performance Evaluation

We consider a learning-based strategy to evaluate FB-MOAC on this experiment. For this strategy, we utilize this fact that optimizing the overflow probability decreases the expected latency according to Equation (36). Consequently, we apply the baseline RL algorithms PPO (Schulman et al., 2017a) and A2C (Grondman et al., 2012) to obtain an offloading policy. We call the resulting policies of these approaches F-PPO and F-A2C, as these algorithms manage the backward reward using a forward mechanism.

Figure 6 reports the histograms (i.e., the empirical probability density function) for the performance of FB-MOAC, F-PPO and F-A2C algorithms (respectively) in terms of r_{CT} and r_{OP}. Clearly, both the forward and backward rewards of FB-MOAC are higher than those of F-PPO and F-A2C approaches. Consequently, FB-MOAC outperforms F-PPO and F-A2C from the perspectives of both expected computation time r_{CT} and overflow probability r_{OP}. In other words, the resulting policy of FB-MOAC Pareto-dominates the

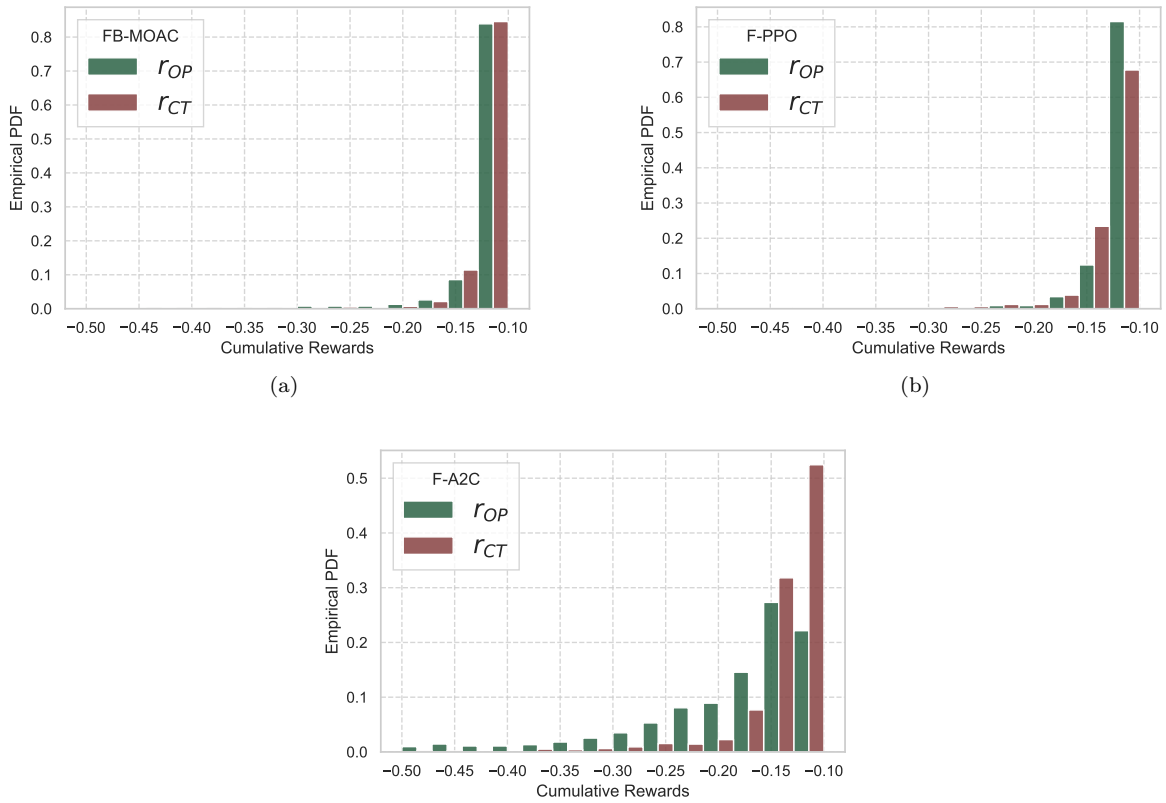

Figure 6: Histograms depicting the empirical distribution function of the computation time r_{CT} and the overflow probability r_{OP} for: (a) FB-MOAC, (b) F-PPO, and (c) F-2AC.

strategies of F-A2C and F-PPO on average. As expected, FB-MOAC shows a more significant improvement in the computation time compared to the other two algorithms. Nonetheless, FB-MOAC even gives a better overflow probability performance than that of F-A2C and F-PPO due to developing a more favorable learning mechanism even for the forward dynamics. These results indicate the importance of explicitly incorporating the backward MDP rather than eliminating it through adjustments to the backward rewards. They also demonstrate the effectiveness of the proposed FB-MOAC algorithm in addressing the corresponding FB-MDP problem.

E Deriving Pareto-optimal Solutions

Here, we employ the mechanism explained in Section 4.3 to obtain the Pareto-optimal solutions of the use case considered in Section 5.2, namely, edge caching in wireless networks. Figure 7 illustrates the collection of Pareto-optimal solutions with diverse preference parameters $\epsilon_i^f \in [0.1, 1]$ and $\epsilon_i^b \in [0.1, 1]$. Note that most of the solutions cannot be dominated by others, therefore, FB-MOAC can provide most of the Pareto-optimal solutions with the proposed preference policy.

E.1 Transforming a FB-SDE into a FB-MDP

This section shows the wider applicability of FB-MDPs and FB-MOAC to problems described by FB-SDEs. Specifically, it explains a general method to transform a FB-SDE into a FB-MDP, which can then be solved with FB-MOAC (as described in Section 5.1). In particular, the Euler-Maruyama method (Kloeden & Platen,

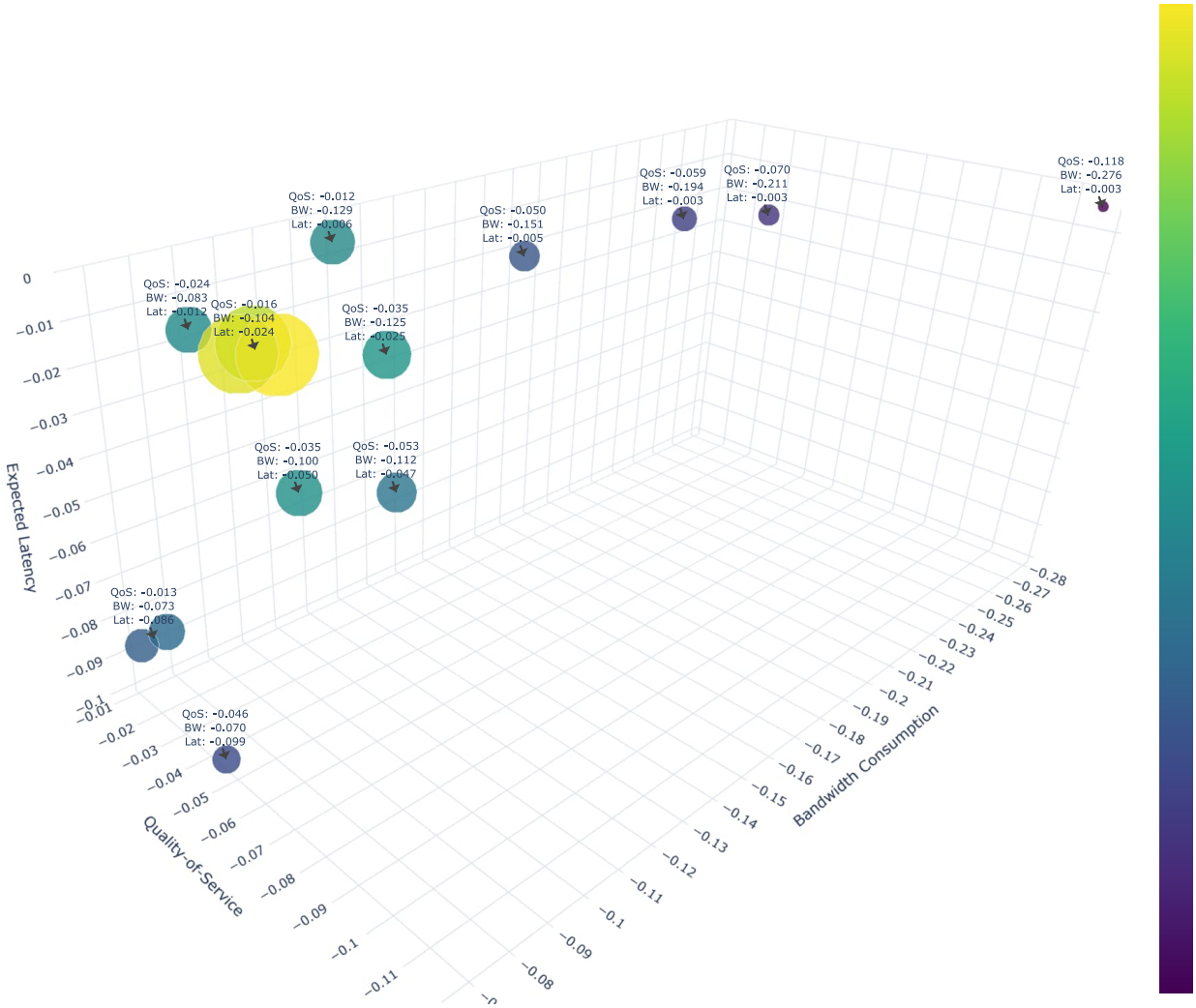

Figure 7: The collection of Pareto-optimal solutions for the use case of edge caching, obtained by applying a discrete policy over different preference settings $\epsilon_i^f \in [0.1, 1]$ and $\epsilon_i^b \in [0.1, 1]$. The radius of the points denotes the probability of occurrence. Given that many of these solutions cannot be dominated by others, the FB-MOAC algorithm can efficiently provide the Pareto-front solutions.

1992) can be used to discretize the space of control problems. More specifically, the forward and backward SDEs can be transformed to forward and backward MDPs, respectively.

Consider the following controlled FB-SDE:

$$\begin{cases} d\mathbf{x}(t) = \boldsymbol{f}(\mathbf{x}(t), \mathbf{u}(t), t)\, dt + \sum_{i=1}^{l} \boldsymbol{\sigma}^i(\mathbf{x}(t), \mathbf{u}(t), t)\, dw^i(t), \\ d\mathbf{y}(t) = \boldsymbol{g}(\mathbf{y}(t), \mathbf{u}(t), \{\mathbf{z}^i(t)\}_i, t)\, dt + \sum_{i=1}^{l} \mathbf{z}^i(t)\, dw^i(t), \\ \mathbf{x}(0) = x_0, \quad \mathbf{y}(T) = y_T, \end{cases} \tag{37}$$

where $\mathbf{w}(t) = \{w^i(t)\}_{i=1}^{l}$ is an l-dimensional Wiener process, $\mathbf{x}(t) \in \mathbb{R}^n$ is the forward process, $\boldsymbol{f}(\cdot,\cdot,\cdot) : \mathbb{R}^n \times U \times [0,T] \to \mathbb{R}^n$ is the drift function which describes the dynamics of the forward SDE and is governed by an optimization control process $\mathbf{u}(t) \in U \subset \mathbb{R}^k$, and $\boldsymbol{\sigma}^i(\cdot,\cdot,\cdot) : \mathbb{R}^n \times U \times [0,T] \to \mathbb{R}^n$ is the diffusion coefficient determining the extent of noise added to the forward dynamics. Conversely, $\mathbf{y}(t) \in \mathbb{R}^m$ is the backward process, $\boldsymbol{g}(\cdot,\cdot,\cdot,\cdot) : \mathbb{R}^m \times U \times \mathbb{R}^{m\times n} \times [0,T] \to \mathbb{R}^m$ is the generator function and $\mathbf{z}^i(t) \in \mathbb{R}^m$ is the dynamics control process.

Note that the solution of the backward SDE is determined by the pair $(\mathbf{y}(\cdot), \{\mathbf{z}^i(\cdot)\}_i)$ where $\{\mathbf{z}^i(\cdot)\}_i$ should be found to guarantee that the backward process $\mathbf{y}(t)$ is properly adapted. The solution of FB-SDE (37) is thus denoted by the tuple $(\mathbf{x}(\cdot), \mathbf{y}(\cdot), \{\mathbf{z}^i(\cdot)\}_i)$.

In this section, we resort to Euler-type numerical approaches, which discretizes the evolution of dynamics, to numerically solve the considered FB-SDE. In this regard, we partition the time interval $[0, T]$ into N sub-intervals $[t_{k-1}, t_k)$ for $k \in \{1, \dots, N\}$, each sub-interval with length $\Delta t = \frac{T}{N}$, where $t_0 = 0$ and $t_N = T$. By applying the Euler–Maruyama method (Kloeden & Platen, 1992), we then obtain:

$$\mathbf{x}(t_k + \Delta t) \approx \mathbf{x}(t_k) + \boldsymbol{f}(\mathbf{x}(t_k), \mathbf{u}(t_k), t_k)\Delta t + \sum_{i=1}^{l} \boldsymbol{\sigma}^i(\mathbf{x}(t_k), \mathbf{u}(t_k), t_k)\Delta w^i(t_k), \quad \text{for } k \in \{0, \dots, N-1\} \tag{38}$$

where $\Delta w^i(t_k) = w^i(t_k + \Delta t) - w^i(t_k)$ is a Gaussian random variable with variance Δt. (38) can be interpreted as a forward MDP with action $\mathbf{u}(\cdot)$ and forward state $\mathbf{x}(\cdot)$.

For the backward SDE, we exploit a *semi-stochastic approach* (Archibald & Yong, 2020). Although, this might lead to more iterations for the algorithm to converge to an accurate solution, it is considerably more efficient from the complexity perspective. This can be compared with the stochastic gradient descent that alleviates the extreme complexity of gradient descent by estimating the expectation with a single sample. Accordingly, we can get:

$$\mathbf{y}(t_k) \approx \mathbf{y}(t_k + \Delta t - \mathbf{g}(\mathbf{y}(t_k + \Delta t), \mathbf{u}(t_k + \Delta t), \mathbf{Z}(t_k + \Delta t), t_k + \Delta t)\, \Delta t. \tag{39}$$

where $\mathbf{Z}(\cdot) = \{\mathbf{z}^i(\cdot)\}_{i=1}^l$, and $\mathbf{z}^i(t)$ is obtained by

$$\mathbf{z}^i(t_k) \approx \frac{1}{\Delta t}\mathbf{y}(t_k + \Delta t)\, \Delta w^i(t), \qquad \text{for } i \in \{1, \dots, l\}. \tag{40}$$

Equation (39), accompanied with Equation (40), represents a backward MDP with action $(\mathbf{u}(\cdot), \mathbf{Z}(\cdot))$ and backward state $\mathbf{y}(\cdot)$.